The response of the Walker circulation to Last Glacial Maximum forcing: Implications for detection in proxies

P. N. DiNezio,[1] A. Clement,[1] G. A. Vecchi,[2] B. Soden,[1] A. J. Broccoli,[3]
B. L. Otto-Bliesner,[4] and P. Braconnot[5]

Received 19 November 2010; revised 20 May 2011; accepted 2 June 2011; published 26 August 2011.

[1] The response of the Walker circulation to Last Glacial Maximum (LGM) forcing is analyzed using an ensemble of six coordinated coupled climate model experiments. The tropical atmospheric overturning circulation strengthens in all models in a manner that is dictated by the response of the hydrological cycle to tropical cooling. This response arises from the same mechanism that has been found to explain the weakening of the tropical circulation in response to anthropogenic global warming but with opposite sign. Analysis of the model differences shows that the ascending branch of the Walker circulation strengthens via this mechanism but vertical motion also weakens over areas of the Maritime Continent exposed due to lower sea level. Each model exhibits a different balance between these two mechanisms, and the result is a Pacific Walker circulation response that is not robust. Further, even those models that simulate a stronger Walker circulation during the LGM do not simulate clear patterns of surface cooling, such as La Niña-like cooling or enhanced equatorial cooling, as proposed by previous studies. In contrast, the changes in the Walker circulation have a robust and distinctive signature on the tilt of the equatorial thermocline, as expected from zonal momentum balance. The changes in the Walker circulation also have a clear signature on the spatial pattern of the precipitation changes. A reduction of the east-west salinity contrast in the Indian Ocean is related to the precipitation changes resulting from a weakening of the Indian Walker circulation. These results indicate that proxies of thermocline depth and sea surface salinity can be used to detect actual LGM changes in the Pacific and Indian Walker circulations, respectively, and help to constrain the sensitivity of the Walker circulation to tropical cooling.

Citation: DiNezio, P. N., A. Clement, G. A. Vecchi, B. Soden, A. J. Broccoli, B. L. Otto-Bliesner, and P. Braconnot (2011), The response of the Walker circulation to Last Glacial Maximum forcing: Implications for detection in proxies, *Paleoceanography*, *26*, PA3217, doi:10.1029/2010PA002083.

1. Introduction

[2] A weakening of the Walker circulation in response to anthropogenic global warming (AGW) is expected from theory and numerical simulations [*Held and Soden* 2006; *Vecchi et al.*, 2006; *Vecchi and Soden*, 2007a]. Simulations with coupled general circulation models (GCMs) and analogies with observed climate variability suggest that this response could result in patterns of regional climate change over the tropical Pacific and beyond, with impacts on regional precipitation patterns [*Seager et al.*, 2005], fisheries [*Bakun and Weeks*, 2008], and Atlantic hurricanes [*Vecchi and Soden*, 2007b]. GCM projections are consistent with observations, which exhibit a 3.5% reduction in the east-west sea level pressure (SLP) gradient on the equatorial Pacific during the 1854–2005 period [*Vecchi et al.*, 2006].

[3] According to the mechanism proposed by *Held and Soden* [2006] and *Vecchi and Soden* [2007a] (hereafter HSV mechanism), as the tropics warm, boundary layer humidity increases more than does precipitation, and a reduction in circulation is required to maintain a balanced flow of water vapor entering areas of convection. Thus, the resulting weakening of tropical circulation (including the ascending branch of the Walker circulation) depends on the sensitivity of global mean precipitation to warming, which is not well constrained by observations [*Wentz et al.*, 2007; *Liepert and Previdi*, 2009].

[4] Records from past climates provide an opportunity to test the model simulations of Walker circulation changes. The

[1]Division of Meteorology and Physical Oceanography, RSMAS, University of Miami, Miami, Florida, USA.
[2]Geophyscial Fluid Dynamics Laboratory, NOAA, Princeton, New Jersey, USA.
[3]Department of Environmental Sciences, Rutgers University, New Brunswick, New Jersey, USA.
[4]Climate Change Research Section, CCR/CGD, NCAR, Boulder, Colorado, USA.
[5]IPSL, Laboratoire de Sciences du Climat et de l'Environnement, CEA Saclay, Gif-sur-Yvette, France.

0883-8305/11/2010PA002083

tropics were cooler during the Last Glacial Maximum (LGM), about 21,000 years ago; thus, records from this period could be used to test the hypothesis that the Walker circulation *strengthens* via the HSV mechanism as the tropics cool (i.e., the opposite to a weakening in response to warming). Changes in the Walker circulation during the LGM have been previously inferred from spatial patterns in ocean surface temperature change derived from microfossil distributions and their geochemical composition through an analogy with El Niño/Southern Oscillation (ENSO) [e.g., *Andreasen and Ravelo*, 1997; *Andreasen et al.*, 2001; *Koutavas et al.*, 2002]. Such an analogy is generally invoked through the following reasoning: If the eastern Pacific were, for example, to cool more than the west in response to forcing by glacial boundary conditions, this would drive stronger Walker circulation, stronger upwelling, and a strengthened thermocline tilt, all of which would act to cool the eastern Pacific and strengthen the Walker circulation. This positive feedback loop is crucial to the growth of El Niño and La Niña events and is known as the "Bjerknes feedback."

[5] However, based on current paleoproxy climate reconstructions, it is not clear whether the LGM tropics is best described as either El Niño- or La Niña-like. Proxies of sea surface temperature (SST) based on planktonic microfossils distributions calibrated with a methodology that avoids the no-analog problem suggest La Niña-like cooling of 5–6 K in the eastern equatorial Pacific [*Mix et al.*, 1999]. The stronger zonal SST gradient suggested by this study is consistent with estimates of a stronger thermocline tilt [*Andreasen and Ravelo*, 1997], suggesting a stronger Walker circulation during the LGM. However, Mg/Ca ratios in planktonic microfossils suggest either a weaker [*Koutavas et al.*, 2002] or stronger [*Lea et al.*, 2000] zonal SST gradient. Because the change in the east-west gradient is not robust among the different methodologies, a clear El Niño- or La Niña-like signature is not evident in a recent multiproxy synthesis [*MARGO Project Members*, 2009]. Coupled GCM experiments also simulate a range of responses in the equatorial SST gradient, from weaker [*Otto-Bliesner et al.*, 2003], unaltered [*Otto-Bliesner et al.*, 2009], to stronger [*Rosenthal and Broccoli*, 2004] equatorial SST gradients.

[6] The second phase of the Paleoclimate Modeling Intercomparison Project (PMIP2) has coordinated the first set of LGM experiments using coupled GCMs forced with a standard set of forcing and boundary conditions [*Braconnot et al.*, 2007]. These experiments offer the possibility of studying mechanisms of LGM climate change without the discrepancies introduced by differing forcing or boundary conditions. Moreover, each individual model represents an independent realization of the LGM climate, thus allowing the study of the robustness of the different climate responses. However, these LGM experiments do not agree in many aspects of the signature of the SST changes in the Pacific, such as the equatorial gradient and the enhanced cooling in the south Pacific (Figure 1b). The lack of agreement is noteworthy because (1) all coupled GCMs participating in PMIP2 use the same LGM boundary conditions (external forcing) and (2) the same models agree in the response to 2xCO2 forcing (Figure 1a).

[7] Here we will analyze the different mechanisms simulated by the PMIP2 models along with their link with observable aspects of the LGM climate response. We categorize these mechanisms as those that lead to robust responses and those that are responsible for intermodel differences (see section 2.3 for more details on the definition of robustness). The robust mechanisms are interpreted to be independent of intermodel differences in the representation of the climate system, thus attributable to fundamental physical principles. For these mechanisms, our current level of understanding of the climate system warrants looking for their signature in proxies. Moreover, robust responses could help bridge controversies between different proxy methodologies or guide the development of new proxies. Conversely, we also attribute the origin of intermodel differences and provide recommendations for constraining uncertainty in the associated mechanisms using proxies.

[8] The organization of this paper is as follows: section 2 presents the coupled GCM experiments; section 3 analyses the response of the tropical atmospheric circulation to both tropical cooling and warming; section 4 describes the changes in the Indo-Pacific Walker circulation in response to LGM forcing and attributes the robust changes and the intermodel differences; section 5 analyses the different ocean responses to the changes in the Walker circulation with emphasis on which proxies can show unambiguous signatures of these changes; and section 6 concludes with a summary of the mechanisms simulated by the GCMs, implications for detection of the signature of these mechanisms in proxies, and ideas for future model-data comparisons.

2. Climate Models and Climate Change Experiments

[9] In this study we compare the time mean climate of the tropical Indo-Pacific simulated by six coupled GCMs in response to (1) forcing and boundary conditions representing of drivers of LGM climate and (2) an idealized AGW experiment forced by doubling atmospheric CO_2 concentrations (2xCO2). The coupled GCMs contributing to PMIP2 are nearly the same model versions that were used to perform the 2xCO2 experiments coordinated by Coupled Model Intercomparison Project phase 3 (CMIP3) (see Table 1 for details). Both projects coordinated preindustrial climate experiments forced with the preindustrial radiative forcing due GHG concentrations, recommended to be prescribed to 280 ppm for CO_2 and 760 ppb for CH_4 in PMIP2. (Models used slightly different CH_4 values for the CMIP3 control experiment. The PMIP2 control experiment used the value for 1750.) The differences between both control climates, 0k_oa (PMIP2) and picntrl (CMIP3), are much smaller than the respective climate changes in response to LGM and 2xCO2 forcing. However, due to slight differences in the models we compute the LGM and 2xCO2 climate changes by subtracting the annual mean climatology of the corresponding control experiment from the annual mean climatology of each of the perturbation experiments (LGM and 2xCO2).

2.1. LGM experiments

[10] Five out of the six LGM experiments were performed for the PMIP2 project (Table 1) with the remaining experiment performed using the CM2.1 model [*Delworth et al.*, 2006], also following the PMIP2 experimental protocol. The initial state in CM2.1 is from a preindustrial control run. Detailed descriptions of the models can be found on the PMIP2 web site (http://pmip2.lsce.ipsl.fr/pmip2/), the Program

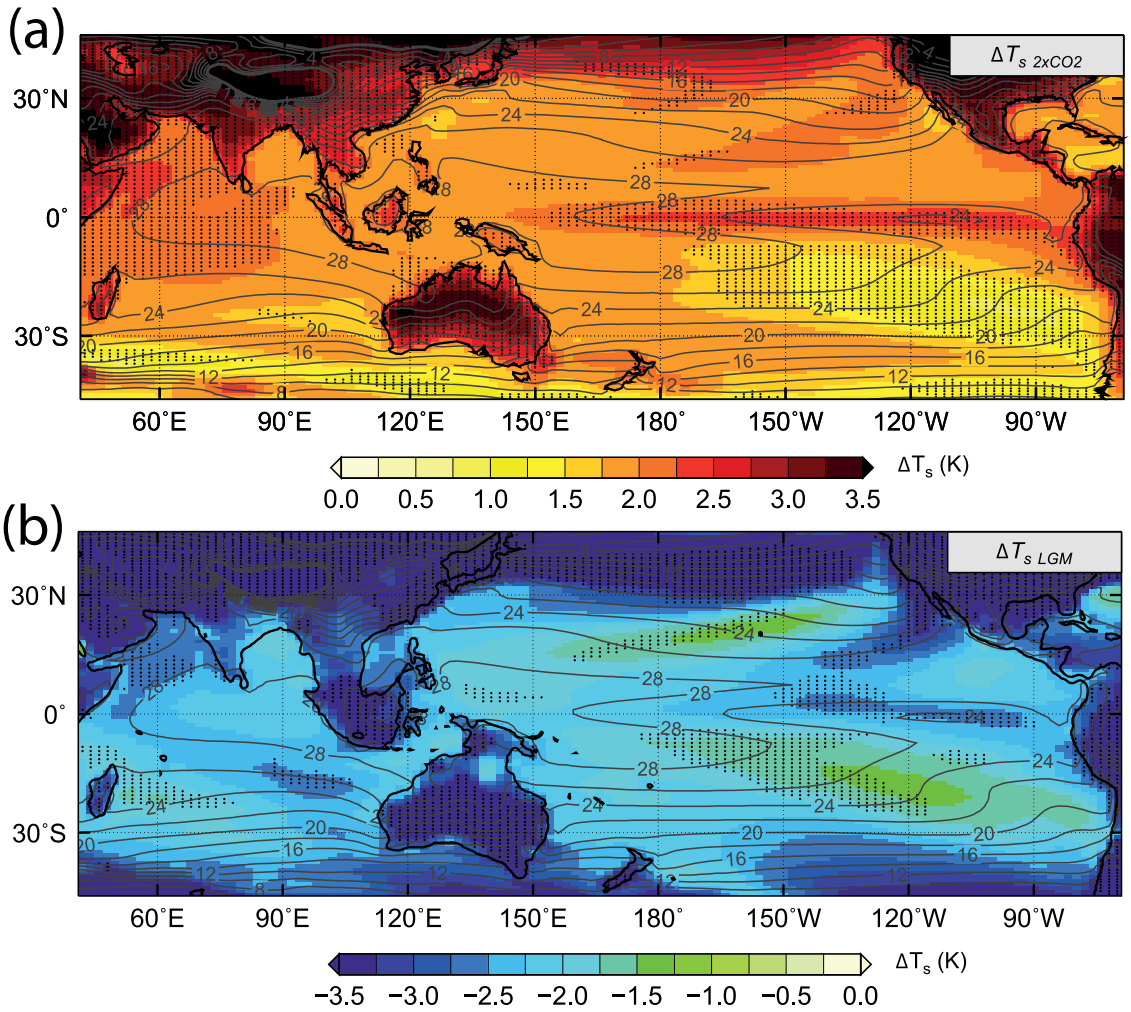

Figure 1. Annual surface temperature change in response to 2xCO2 and LGM forcing. Multimodel mean change in surface temperature (T_s) simulated by six coupled general circulation models (GCMs) in response to (a) doubling of atmospheric CO_2 (2xCO2) and to (b) LGM forcing. Values over the ocean correspond to sea surface temperature (SST). In this and all subsequent figures, the 2xCO2 (LGM) climate change is computed by differencing the annual mean climatology from the 1pctto2x (21k_oa) experiment minus the annual mean climatology from the picntrl (0k_oa) experiment. The multimodel mean change is the averaged climate change across all models. The 2xCO2 climatology corresponds to a quasi-equilibrated 100 year period 50 years after CO_2 doubling. To evaluate the robustness of the pattern of change, the tropical (30°S–30°N) mean change for each model is subtracted from the local change for that model to yield a departure from the tropical mean change. Stippling indicates where all six models agree in the sign of the departure from the tropical mean change. Contours show multimodel annual mean T_s simulated in the respective control experiments. The contour interval (CI) is 2°C.

for Climate Model Diagnosis and Intercomparison (PCMDI) web site (http://www-pcmdi.llnl.gov/ipcc/about_ipcc.php), or in the references listed in Table 1. For the PMIP2 LGM simulations, all of the models used the same forcing and boundary conditions: (1) reduced greenhouse gas (GHG) concentration, (2) insolation changes due to the orbital configuration 21,000 years before present (almost negligible) in the annual mean, (3) surface albedo changes due to prescribed ice sheets and corresponding roughness length, (4) orography changes due to prescribed ice sheets, and (5) changes in land–sea distribution and altitude due to lower sea level during the LGM (about 120 m). Some of the groups also considered changes in the routing of river runoff resulting from the presence of the ice sheets. The mass balance over the ice sheet is also considered by routing extra snow accumulation to the ocean, mimicking iceberg discharge. The LGM experiments analyzed here do not include interactive models representing ice sheets, vegetation, or the carbon cycle. These three components of the climate system are prescribed in each the different experiments. Despite evidence of large vegetation changes during the LGM [e.g., *Farrera et al.*, 1999], vegetation is prescribed to be the same as in the control simulation (0k_oa), except for the regions covered by ice sheets or exposed due to the LGM sea level drop.

[11] Only the six GCMs analyzed here submitted all the atmosphere and ocean variables required by our analysis. For these variables, the model output is available as climatological

Table 1. Models With LGM and 2xCO2 Simulations Coordinated by the PMIP2 and CMIP3 Projects, Respectively

Model	Reference	Institution, Country	Model Resolution		Differences From 2xCO2 Experiment
			Atmosphere Lat × Long	Ocean Lat × Long	
FGOALS-g1.0	*Yu et al.* [2004]	LASG/Institute of Atmospheric Physics, China	T42 L26 (2.8° × 2.8°)	1° × 1° L33	None
MIROC3.2	*Hasumi and Emori* [2004]	Center for Climate System Research (University of Tokyo), National Institute for Environmental Studies, and Frontier Research Center for Global Change (JAMSTEC), Japan	T42 L20 (2.8° × 9 2.8°)	0.5–1.4° × 1.4° L43	None
CCSM3.0	*Otto-Bliesner et al.* [2006a, 2006b]	National Center for Atmospheric Research, United States	T42 L26 (2.8° × 2.8°)	1/3°–1° × 1° L40	CMIP3 simulations use atmospheric model resolution: T85 L26
IPSL-CM4	*Marti et al.* [2010]	Institut Pierre Simon Laplace, France	2.5° × 3.75° L19	1–2° × 2° L31	None
HadCM3M2	*Gordon et al.* [2000]	UK Met Office Hadley Centre, United Kingdom	2.5° × 3.75° L19	1.25° × 1.25° L20	CMIP3 simulations use different land surface scheme
GFDL-CM2.1	*Delworth et al.* [2006]	NOAA Geophysical Fluid Dynamics Laboratory, United States	2° × 2.5° L24	1/3°–1° × 1° L50	None

seasonal cycles in the PMIP2 database. These seasonal cycles are computed from the last 50 or 100 year means of the simulations after each model spin-up process. For each variable, we compute the LGM climate change by subtracting the annual mean climatology from the 21k_oa experiment from the annual mean climatology from the 0k_oa experiment. For CCSM3.0, the climatology of 3-D ocean variables (potential temperature, salinity, and velocity) are 10 year monthly means in the PMIP2 database; thus, the results from this model could be more strongly influenced by decadal variability than those in other models. In some models, transients due to the long deep ocean adjustment may still influence the climatologies; however, we only focus on the upper ocean in the study, where we expect the LGM changes to be heavily influenced by the surface forcing, with minor influence from changes in the deep ocean. The initial state of the ocean is taken from a previous LGM simulation for CCSM3.0 [*Shin et al.*, 2003] and HadCM3M2 [*Hewitt et al.*, 2003]. For MIROC3.2 and IPSL-CM4 the initial ocean states are taken from preindustrial spinup runs and integrated for about 500 years. The length of these integrations is too short for a complete ocean adjustment; thus, the deep ocean could not be fully equilibrated.

[12] The LGM boundary conditions are basically the same for all six models, but with some variation in the oceanic part and the land mask. MIROC 3.2 used a present-day ocean bathymetry, coastline, and land mask for the LGM experiment; thus, in this model the Bering Strait is open and no changes in land over the Maritime continent are imposed. All other models have a closed Bering Strait and increased land surface over the Maritime continent to include the effect of lowered sea level. During the LGM the ocean was about 1 psu saltier due to reduced ocean volume, i.e., sea level drop. Not all PMIP2 participants applied this boundary condition. The CCSM3.0 LGM experiment has this salinity rise because the ocean initial state is taken from a previous version simulation. GFDL-CM2.1 also had a 1 psu salinity rise. No salinity rise is applied in the simulations with the remaining models. We removed the global mean salinity rises from the LGM climatology of each model in order to be able to compare patterns of sea surface salinity (SSS) among models.

2.2. The 2xCO2 Experiments

[13] Sensitivity experiments forced with each of the LGM boundary conditions separately were not run for PMIP2 due to the computing cost of running several equilibrated experiments. In this study, we use the 2xCO2 experiments in order to guide the attribution of the LGM changes due to reduced GHGs during the LGM, assuming that the responses to each of the different LGM forcing are linear. For instance, the 2xCO2 experiments are very useful to interpret the response of the ascending branch of the Walker circulation in the LGM experiments because the atmospheric circulation in this region is expected to be influenced by changes restricted to the tropics, such as patterns in surface cooling or changes in exposed land due to lower sea level, with a negligible influence from the orographic forcing of the Laurentide ice sheet.

[14] The 2xCO2 experiments coordinated by CMIP3 are started from the control experiments (picntrl), increasing CO_2 concentrations at a rate of 1% yr^{-1}, from preindustrial CO_2 concentrations (280 ppm), until doubling at 560 ppm on year 71. These experiments were run for at least 150 additional years with constant CO_2 concentrations of 560 ppm. To

minimize the influence of transient warming during the first 71 years of the experiments, we compute a quasi-equilibrated 2xCO2 climate using the last 100 years of this experiment (50 years after CO_2 is doubled). However, these models still have warming trends of less than 0.4 K per century during the last 100 years, which are too small to change our conclusions about the climate response. A fundamental difference between AGW and LGM is expected in the deep ocean. Due to the much faster nature of AGW, the deep ocean does not warm as fast as the upper ocean; thus, most of the warming occurs above the thermocline. In contrast, during the LGM the deep ocean had time to equilibrate with the surface cooling and this needs to be represented in numerical simulations; hence the requirement of very long ocean spin-up.

2.3. Robustness

[15] Throughout this study we focus on those aspects of the climate response that appear in the multimodel mean. To provide an indication of how robust these signals are across the different models, we also indicate where all six models agree with the sign of the multimodel mean change (e.g., Figure 3, stippled areas). This estimate of robustness does not provide information about how close the model responses are to the multimodel mean and thus is unable to detect outliers. However, it remains useful in our study, because much of the debate on the LGM tropics has been on the sign of the change of the Walker circulation (i.e., weaker or stronger). In addition, we analyzed the response by each individual model to avoid making invalid conclusions from the multimodel mean.

[16] A similar definition of robustness is used for variables with changes of a given sign, such as SST and SLP. For these variables we are interested in quantifying the robustness of the spatial patterns of the change, independent of the magnitude of the tropical mean cooling or warming. To evaluate the robustness of the patterns of change, the tropical (30°S–30°N) mean change for each model is subtracted from the local change for that model, to yield a departure from the tropical mean change. Thus, the SST and SLP changes are robust where all six models agree with the sign of the departure from the tropical mean change (e.g., Figures 1 and 2, stippled areas).

3. Robust Responses of the Tropical Atmospheric Circulation

[17] The changes in SLP reveal some important differences between the response of the atmospheric circulation to 2xCO2 and LGM forcing (Figure 2) that are not so evident in the SST changes (Figure 1). All models simulate a weakened east-west SLP gradient in the Pacific basin in response to 2xCO2 forcing, indicating a robust weakening of the Walker circulation (Figure 2a) [*Held and Soden*, 2006; *Vecchi and Soden*, 2007a]. In contrast, the multimodel mean SLP change in response to LGM forcing shows a stronger east-west SLP gradient in the Pacific (consistent and opposite to the response to 2xCO2), but not all six models simulate this response (note that almost the entire equatorial Indo-Pacific is not stippled in Figure 2b). Analysis of the individual response indicates that four (FGOALS-g1.0, MIROC3.2, CCSM3.0, IPSL-CM4) out of the six models show a stronger east-west SLP gradient shown by the multimodel mean SLP change. The SLP responses of the remaining two models (HadCM3M2, GFDL-CM2.1) exhibit no change in the east-west gradient.

[18] The multimodel changes in midtropospheric vertical velocity, ω_{500} (Figure 3), show simulated changes in the tropical atmospheric overturning circulation that are consistent with the SLP changes. (We use the vertical velocity in pressure coordinates at the 500 hPa level ω_{500} because this level is where the convergent motion in the boundary layer has the strongest effect in vertical motions in the free troposphere. Figure 5 shows that the results are insensitive to the use of other midtropospheric levels.) The robust ω_{500} changes in response to 2xCO2 (Figure 3a) show a decrease in ascending motion over the WPWP, a region of ascending motion, and a decrease in subsidence over the central and eastern equatorial Pacific a region of subsidence in the control climate. Note that ω is a vertical velocity in pressure coordinates; thus, the ascending motion is negative. These changes are consistent with the HSV mechanism, which predicts a decrease in ascending motion ($\Delta\omega_{500} > 0$) in regions of ascent ($\omega_{500} < 0$) as the tropics warm up.

[19] Due to cooler tropics, the HSV mechanism predicts the opposite response for the LGM: an increase in ascending motion ($\Delta\omega_{500} < 0$) in regions of ascent, i.e., a strengthening of the tropical overturning atmospheric circulation. The HSV mechanism requires that the acceleration of tropical overturning circulation be proportional to the background circulation (as is largely the case in models of AGW). However, the multimodel mean change in midtropospheric vertical velocity does not show robust increased ascending motion ($\Delta\omega_{500} < 0$) over the WPWP as predicted by this mechanism (Figure 3b). Moreover, according to this, upward motion should also intensify in the Intertropical Convergence Zone (ITCZ). However, the changes in ω_{500} show anomalous subsidence there, which is likely the result of the equatorward shift of the North Pacific subtropical high.

[20] Unlike the AGW experiments, the models simulate the increase in ascending motion required by the HSV mechanism over the off-equatorial regions of ascent, such as the convergence zones in both hemispheres in the western Pacific. This apparent discrepancy is not at odds with the HSV mechanism because the constraint imposed by the differential sensitivity of precipitation and humidity has to be satisfied for the tropics on average, but not locally.

[21] In order to interpret intermodel differences in the response of the tropics to LGM forcing we analyze the changes in the hydrological cycle and in the tropical circulation in each individual model following the methodology presented by *Vecchi and Soden* [2007a]. For both 2xCO2 and LGM, the models simulate a close relationship between the changes in atmospheric water vapor and tropical (30°S–30°N) warming/cooling. The fractional changes in column-integrated water vapor, $\Delta q/q$, and temperature, ΔT_s, exhibit a nearly linear relationship (Figure 4a, red and blue circles are tropical mean 2xCO2 and LGM changes, respectively). In all models and experiments (absolute) humidity changes by 7.5% K^{-1}, which is consistent with changes in saturation vapor pressure from the Clausius–Clapeyron (C–C) equation under constant relative humidity. Tropical precipitation, in contrast, changes at a smaller rate, $\Delta P/P$, of about 1.5% K^{-1} for 2xCO2 and 2.7% K^{-1} for LGM experiments (Figure 4b). The larger intermodel spread in the rate of change of precipitation,

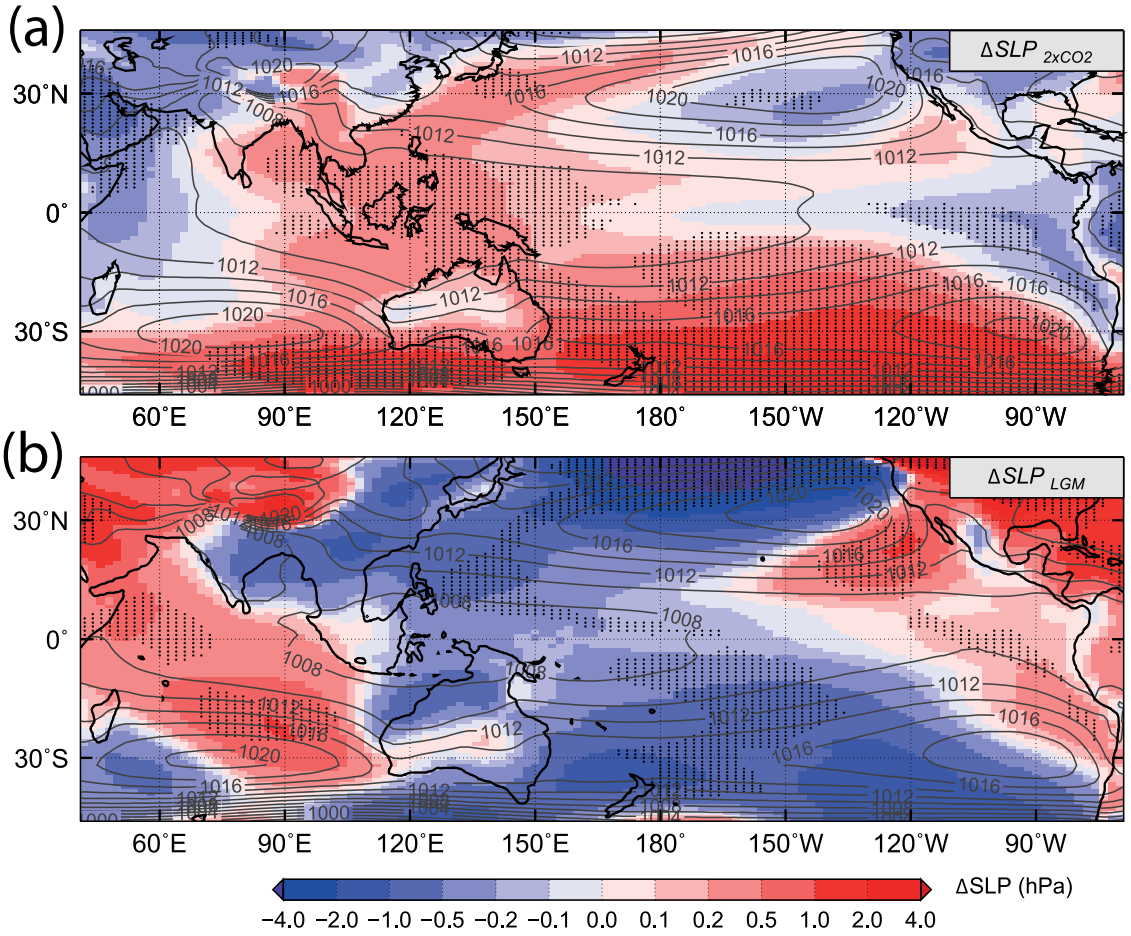

Figure 2. Changes in sea level pressure in response to 2xCO2 and LGM forcing. Multimodel mean change in sea level pressure (SLP) simulated by six coupled general circulation models (GCMs) in response to (a) doubling of atmospheric CO_2 (2xCO2) and to (b) LGM forcing. Note that global mean warming (cooling) results in substantial tropical mean decrease (increase) in SLP with a magnitude larger than that of the spatial patterns. To evaluate the robustness of the pattern of change, the tropical (30°S–30°N) mean SLP change for each model is subtracted from the local change for that model to yield a departure from the tropical mean SLP change. Stippling is as in Figure 1. Contours show multimodel annual mean SLP simulated in the respective control experiments. CI = 2 hPa. Note that the color scale is not linear.

compared with the rate of change of humidity, could be related to differences in the response of clouds, which influence precipitation via changes in the radiation budget of the free troposphere [*Vecchi and Soden*, 2007a].

[22] In all the models, precipitation changes at a smaller rate than the C–C scaling. This differential in the rates of drying (moistening) and precipitation change is a strong constraint on convection in a cooler (warmer) climate because air from the boundary layer entering convective areas is 7.5% drier (wetter), but precipitates at a lesser (large) rate of 2.7% (1.5%) for a tropical mean cooling (warming) of 1K. The differential between the response of precipitation and humidity, $\Delta P/P - \Delta q/q \sim -5\%\ K^{-1}$, is a measure of the changes in the circulation required to satisfy the balance between precipitation and humidity. In other words, the sensitivity of large-scale convection to tropical cooling is given by the differential between the rates of change in precipitation and humidity. This differential constrains the circulation to strengthen by about 5% per degree of tropical mean cooling. An equivalent scaling can be derived for the descending branch of the atmospheric overturning based on the changes in static stability [*Knutson and Manabe*, 1995; *Held and Soden*, 2006].

[23] In all models, the changes in tropical mean atmospheric overturning circulation in response to both LGM and 2xCO2 forcing are consistent with the HSV mechanism. The differential in precipitation and humidity, $\Delta P/P - \Delta q/q$, agrees in magnitude and sign with the fractional change in midtropospheric vertical velocity in regions of ascent, $\Delta\omega^{+}_{500}/\omega^{+}_{500}$ (Figure 4c) suggesting that the robust strengthening of the tropical mean circulation in response to LGM forcing is due to tropical mean cooling. The positive sign in ω^{+}_{500} indicates midtropospheric vertical velocity in regions of ascent. Note that tropical cooling could not only result from reduced GHG forcing, but also from changes in heat transport driven by high latitude cooling [*Broccoli*, 2000]; thus, the stronger LGM atmospheric overturning circulation may be due to both GHG and ice sheet (albedo) forcing.

[24] In all six LGM (2xCO2) experiments the tropical overturning atmospheric circulation strengthens (weakens) in response to tropical cooling (warming) consistent with the

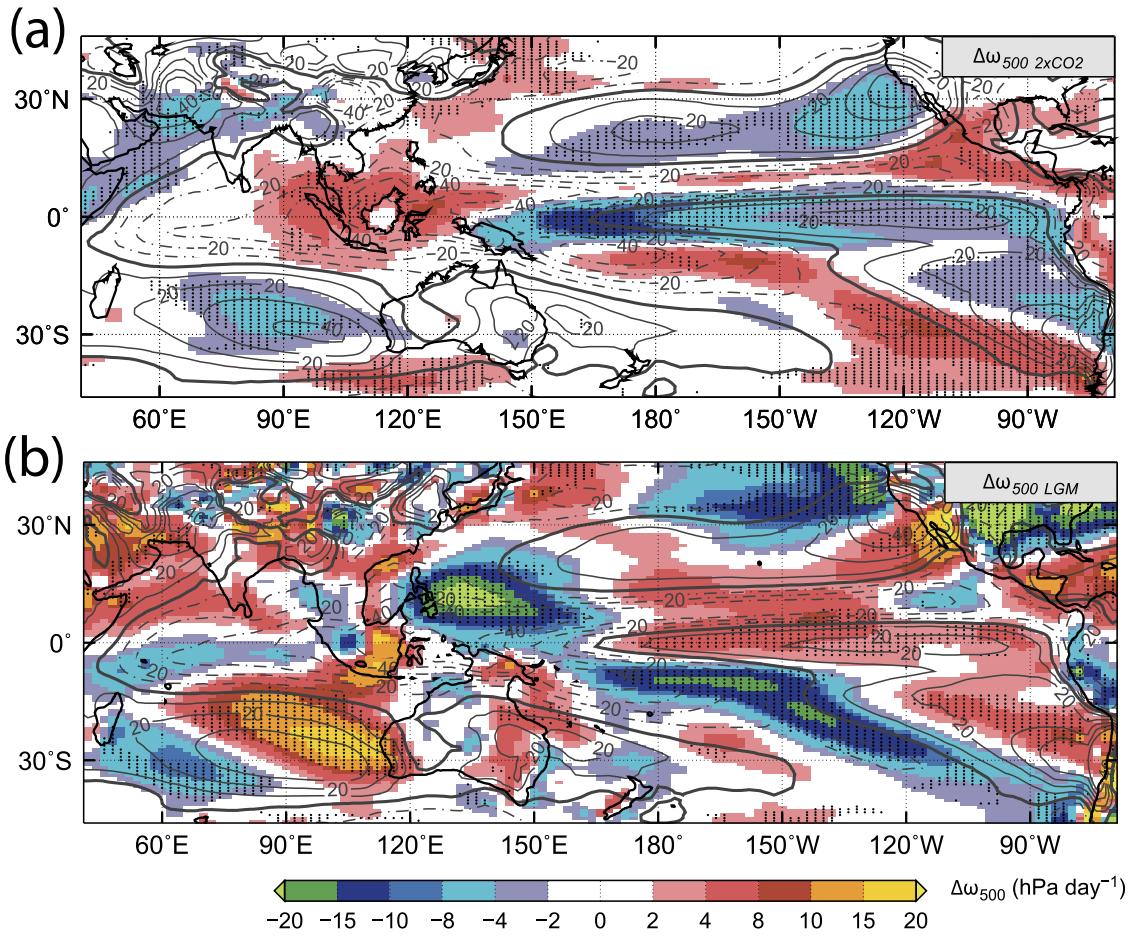

Figure 3. Changes in atmospheric overturning circulation in response to 2xCO2 and LGM forcing. Multimodel mean change in midtropospheric vertical velocity (ω_{500}) simulated by six coupled general circulation models (GCMs) in response to (a) doubling of atmospheric CO_2 (2xCO2) and (b) LGM forcing. Stippling is as in Figure 1. Contours show multimodel annual mean ω_{500} simulated in the respective control experiments. CI = 10 hPa d^{-1}. Note that the color scale is not linear.

HSV mechanism (Figure 4c). In the LGM experiments, the strengthening of the circulation is dominated by a strengthening of the zonally asymmetric component of circulation (Walker), with the strength zonally averaged (Hadley) component of tropical circulation changing relatively less (not shown). The zonally asymmetric component is also the dominant contributor to the weakening of tropical circulation to AGW forcing experiments [e.g., *Held and Soden*, 2006; *Vecchi and Soden*, 2007a]. However, in the LGM experiments, this response does not result in a robust strengthening of the Pacific Walker circulation, as measured by the east-west SLP gradient (dSLP) (Figure 4d). (The east-west SLP gradient (dSLP) is a measure of the strength of the Pacific Walker circulation and is computed as the difference in SLP between a "Tahiti" region (150°W–90°W, 5°S–5°N) minus a "Darwin" region (100°E–180°, 5°S–5°N), as in the Southern Oscillation Index (SOI). Here we define our dSLP index closer to the equator with respect to the conventional SOI definition (10°S–10°N) in order to make sure that the Coriolis effect is negligible and capture changes in the equatorial trade winds more strictly.) The changes in dSLP simulated by FGOALS-g1.0, MIROC3.2, CCSM3.0, and IPSL-CM4 indicate a stronger Pacific Walker circulation (ΔdSLP > 0) in response to LGM forcing. In contrast, HadCM3M2 and GFDL-CM2.1 do not simulate a stronger Pacific Walker circulation (ΔdSLP = 0) despite simulating a stronger overturning circulation. Also note that the fractional changes in convective mass flux ($\Delta P/P - \Delta q/q$), the strength of the ascending branch of the overturning circulation (ω^{+}_{500}), and the Pacific Walker circulation, as measured by the east-west SLP difference, show substantial departures from a one-to-one relationship (diagonal line in Figures 4c and 4d). This suggests that other mechanisms influence the tropical circulation as the climate warms or cools. However, the changes diagnosed following the HSV mechanism agree in sign and order of magnitude, i.e., all models simulate stronger (weaker) overturning of about 10% to 20% as the climate cools (warms). Therefore, the robust part of the changes in the tropical circulation is consistent with the HSV mechanism in all models.

4. Response of the Walker Circulation to LGM Forcing

[25] The response of the Indo-Pacific Walker circulation is more evident in the changes in equatorial vertical velocity, ω_{eq}, as a function of longitude and pressure (Figure 5). The

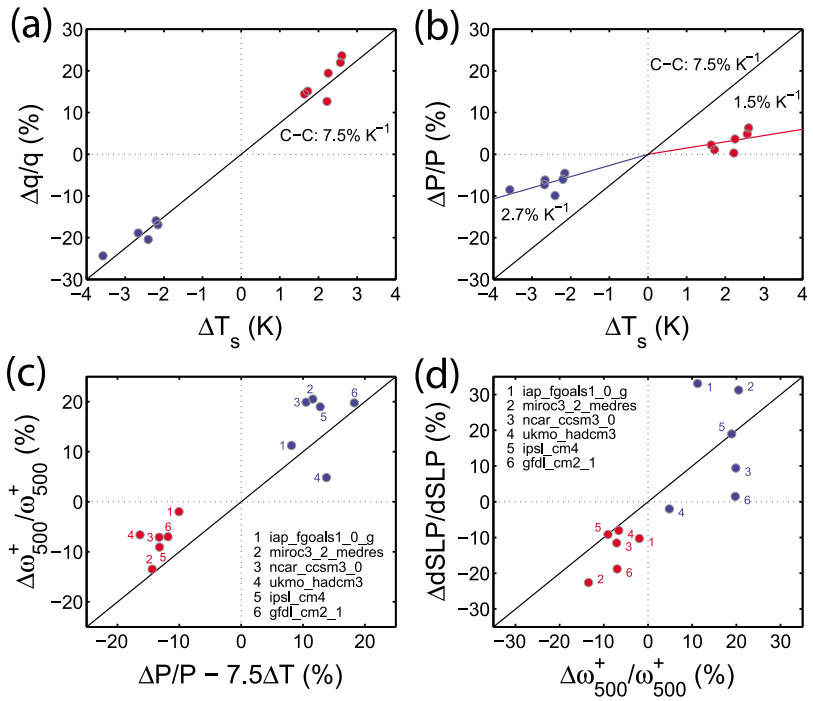

Figure 4. Changes in the hydrological cycle and atmospheric overturning circulation. Tropical mean changes in variables involved in the mechanism used to interpret the changes in the atmospheric overturning circulation simulated by each model in the 2xCO2 (red) and LGM (blue) experiments. (a) Fractional change in column-integrated water vapor ($\Delta q/q$) versus change in surface temperature (ΔTs); (b) fractional change in precipitation ($\Delta P/P$) versus surface temperature (ΔT_s); (c) fractional change in estimated convective mass flux from the scaling between P and q versus fractional change in upward vertical velocity at 500 hPa ($\Delta\omega^+_{500}/\omega^+_{500}$); (d) fractional change in upward vertical velocity at 500 hPa ($\Delta\omega^+_{500}/\omega^+_{500}$) versus fractional change in east-west SLP gradient in the equatorial Pacific (dSLP). In Figures 2a and 2b, the diagonal line is the 7.5% K^{-1} scaling between the fractional change in humidity and temperature determined by the C-C equation assuming constant relative humidity. In Figures 2c and 2d, the diagonal line is the one-to-one scaling between the fractional changes. The dSLP is computed as the difference between a "Tahiti" region (140°W–80°W, 5°S–5°N) minus a "Darwin" region (120°E–180°, 5°S–5°N). The tropical mean changes are computed over the 30°S–30°N latitude band.

models that simulate a stronger SLP gradient in the LGM experiment (FGOALS-g1.0, MIROC3.2, IPSL-CM4, CCSM3.0) exhibit increased ascending motion ($\Delta\omega_{eq} < 0$) over the Maritime Continent and anomalous subsidence ($\Delta\omega_{eq} > 0$) in regions of descending motion over the Pacific and Indian oceans (Figure 5b). In these models the Walker circulation in the Pacific Ocean strengthens in response to LGM forcing, much as it weakens in response to 2xCO2 (Figure 5a). In contrast, HadCM3M2 and GFDL-CM2.1 simulate anomalous subsidence both over the Maritime continent and over the equatorial Pacific Ocean, and increased ascending motion over the Indian Ocean in the LGM experiment (Figure 5c). In these models the Walker circulation weakens in the Indian Ocean and remains unchanged in the Pacific Ocean, as shown by the changes in dSLP (Figure 4d). The anomalous subsidence simulated by these models between 100°E and 120°E coincides with the regions that are set to land in the LGM experiments to represent the changes in land-sea distribution due to lowered sea level. This strongly suggests that changes in sea level during the LGM could have an influence in the Walker circulation.

[26] Analysis of the surface cooling over the Maritime continent in the LGM experiments shows that the regions that are set to land in the LGM experiments exhibit much larger cooling than the surrounding ocean (Figure 6). This anomalous surface cooling could suppress convection either by exceeding the threshold for convection or by generating anomalous temperature gradients with the surrounding ocean, favoring convection over the ocean. In fact, the models that simulate the largest anomalous subsidence over the WPWP, HadCM3M2, GFDL-CM2.1, show the largest cooling over the Sunda shelf, including the Gulf of Thailand, the South China Sea, and the Java Sea. (Figure 6c). In contrast, the models that do not simulate anomalous subsidence over the Sunda shelf, FGOALS-g1.0 and MIROC3.2, exhibit much weaker cooling over exposed land (Figure 6a). This could explain why in these models the ascending branch of the Walker circulation can strengthen via the HSV mechanism without opposition from the suppression of convection over the Sunda shelf. These models simulate the strongest LGM Walker circulation with a ~30% increase in dSLP. CCSM3.0 and IPSL-CM4 fall in between these two responses with respect to both the magnitude of the land cooling (Figure 6b) and the dSLP increase (Figure 4d).

[27] MIROC3.2 used a present-day land mask in the LGM experiment, thus effectively not representing the effect of

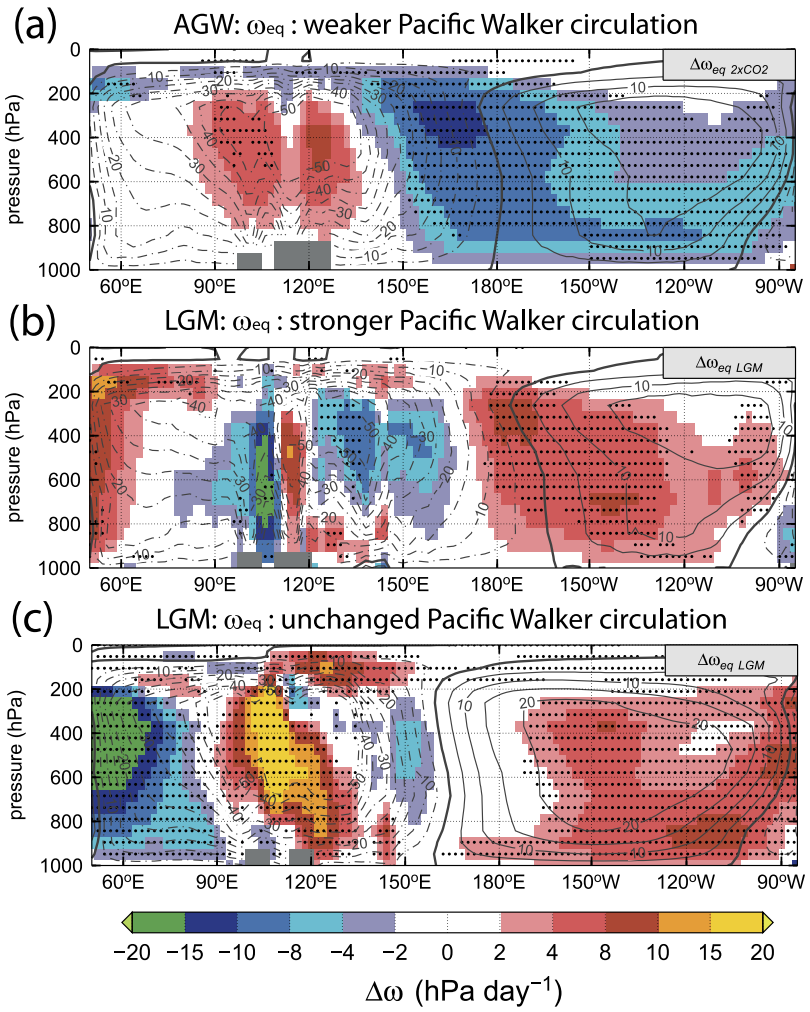

Figure 5. Changes in Indo-Pacific Walker circulation in response to 2xCO2 and LGM forcing. Multimodel mean change in vertical velocity over the equatorial Indo-Pacific (ω_{eq}) simulated by (a) six coupled general circulation models (GCMs) in response to doubling of atmospheric CO_2 (2xCO2), (b) four GCMs that simulate a stronger Walker circulation (ΔdSLP > 0) in response LGM forcing, and (c) two GCMs that simulate an unchanged Walker circulation (ΔdSLP = 0) in response LGM forcing. The equatorial sections are averaged over the 5°S and 5°N latitude band. Stippling is as in Figure 1. Contours show multimodel annual mean ω_{eq} simulated in the respective control experiments. CI = 10 hPa d^{-1}. Note that the color scale is not linear.

lower sea level on the geography of the Maritime Continent. This explains the lack of enhanced cooling over the Sunda shelf. Moreover, in this model the spatial patterns of $\Delta\omega_{500}$ are very similar, but opposite, to the changes in response to 2xCO2 forcing. Moreover, this model does not exhibit any anomalous subsidence over exposed land areas, supporting the hypothesis that the anomalous subsidence is a response to the changes in land-sea distribution. This strongly suggests that in the absence of land-sea distribution changes over the Maritime continent, the Indo-Pacific Walker circulation responds via the same mechanism in both LGM and 2xCO2/AGW experiments, i.e., the HSV mechanism. This also supports the idea that the intermodel differences result from the reduction in convection associated with the changes in land-sea distribution due to lower sea level.

[28] In the remaining models, the intermodel differences in the differential in land-sea cooling could be related to the land surface model. None of these models use interactive vegetation, but the land surface models could have different properties set over the exposed land in this region. For instance, for IPSL-CM4, vegetation from nearby grid point was interpolated onto points over exposed land in order avoid having bare soil areas in the tropics. However, in each model the differential in cooling over the Maritime continent is correlated with the changes in other land areas, such as Australia and South America (not shown). This suggests that the intermodel differences in cooling over the Maritime continent result from general properties of the land surface model, rather than from the representation of the exposed land. Thus, continental proxies from the Southern hemisphere could be used to constrain the simulated cooling over the Maritime continent and improve land-surface models.

[29] The intermodel differences in the response of the ascending branch of the Walker circulation could result

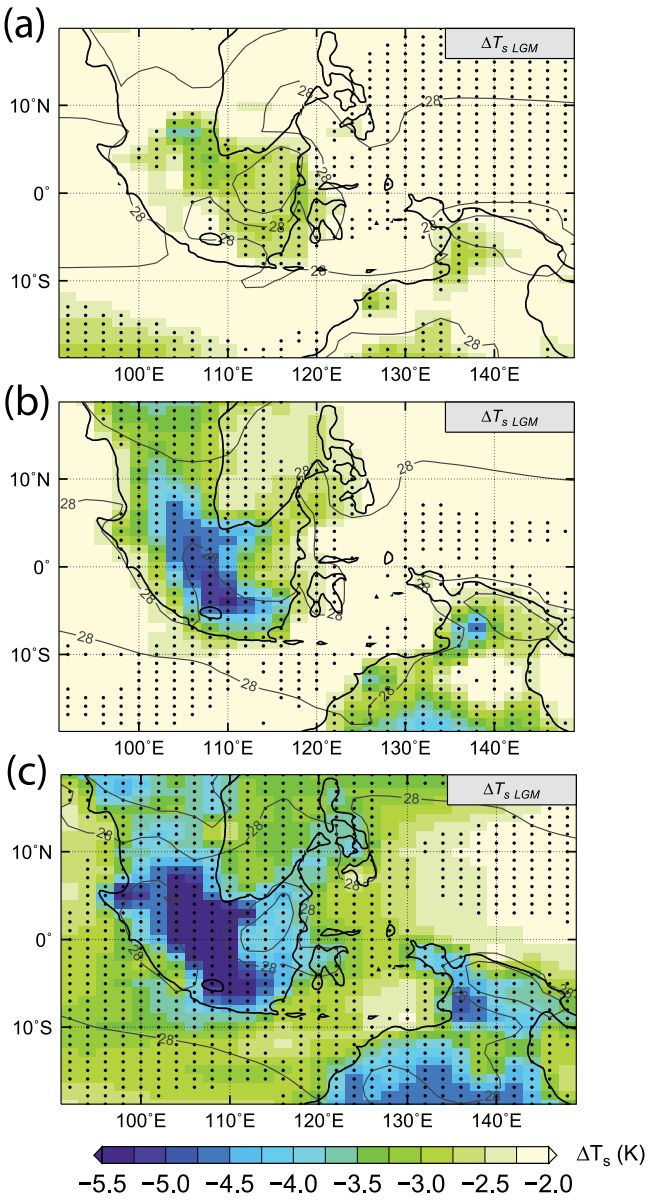

Figure 6. Intermodel differences in cooling over the Maritime Continent. Multimodel mean change in surface temperature simulated by (a) FGOALS-g1.0 and MIROC3.2, (b) CCSM3.0 and IPSL-CM4, and (c) GFDL-CM2.1 and HadCM3M2. Stippling indicates where the models agree in the sign of the changes. Note that the color scale is different from Figure 1b. The coastlines correspond to the 120 m isobath of the present-day ocean bathymetry.

from differences in the simulation of the control climate as well. Current coupled GCMs simulate a cold tongue is too cold and extends excessively westward compared with the Earth's climate. For instance, in both HadCM3M2 and GFDL-CM2.1, models where the Pacific Walker circulation does not strengthen, the subsidence associated with the descending branch of the Walker circulation extends westward (Figure 5c) compared with the models with a stronger LGM circulation (Figure 5b). The $\omega_{eq} = 0$ solid contour that separates the ascending branch ($\omega_{eq} < 0$, dashed contours in Figure 5) from the descending branch ($\omega_{eq} > 0$, solid contours in Figure 5) of the Pacific Walker circulation is located about 160°E in the models with an unchanged circulation (Figure 5c). In contrast, the ascending branch extends eastward to about 160°W in the models with a stronger LGM circulation (Figure 5b).

[30] According to the HSV mechanism, the strengthening of the atmospheric circulation occurs in areas of convection over the ocean where humidity changes follow the C–C relationship. Over the equatorial Pacific, HadCM3M2 and GFDL-CM2.1 simulate almost no ascending motion over the ocean in the control climate. Therefore, the equatorial subsidence, typical of the central and eastern Pacific, extends excessively westward, making the Pacific Walker circulation unsensitive to the HSV mechanism, and allowing the weakening due to the exposure of the Sunda shelf to dominate the response.

[31] To summarize, regional deviations from the constraint in the tropical overturning circulation imposed by the HSV mechanism are possible, but this differential between the precipitation and humidity changes has to be satisfied in the tropical mean, strengthening the tropical mean overturning circulation as a result. All six models simulate changes in ascending motion, as diagnosed by ω^{+}_{500}, consistent with this argument. However, the models achieve this constraint through two possible ways: (1) a stronger ascending branch of the Walker circulation, i.e., $\Delta\omega^{+}_{500} < 0$ over the maritime continent, only in those models where the response of convection to enhanced land cooling is weak, and/or (2) stronger ascending motion, i.e., $\Delta\omega^{+}_{500} < 0$, in the convergence zones off the equator, however, with no impact on the Walker circulation.

[32] In general the models simulate a one-to-one relationship between changes in the east-west SLP gradient and the zonally averaged zonal equatorial wind stress, $\langle \tau^{x} \rangle$ (Figure 7). The changes in Walker circulation drive changes in the surface winds resulting in weaker (Figure 7, red circles; Figure 8a, vectors) and stronger (Figure 7, blue circles; Figure 8b, vectors) equatorial trade winds in the 2xCO2 and LGM experiments respectively. GFDL-CM2.1 and HadCM3M2 do not simulate stronger equatorial trades in

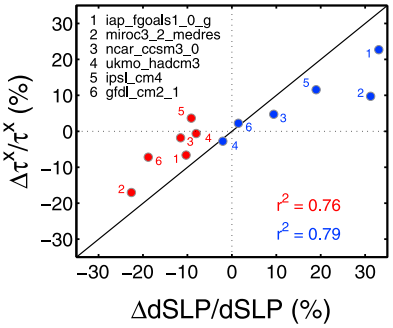

Figure 7. Changes in SLP gradient and zonal trade winds in the equatorial Pacific in response to 2xCO2 and LGM forcing. Fractional change in zonal wind stress averaged over the equatorial Pacific (2°S–2°N) versus changes in sea level pressure gradient, as diagnosed by the east-west SLP difference (SLP), simulated by each model in response to 2xCO2 (red) and LGM (blue) forcing.

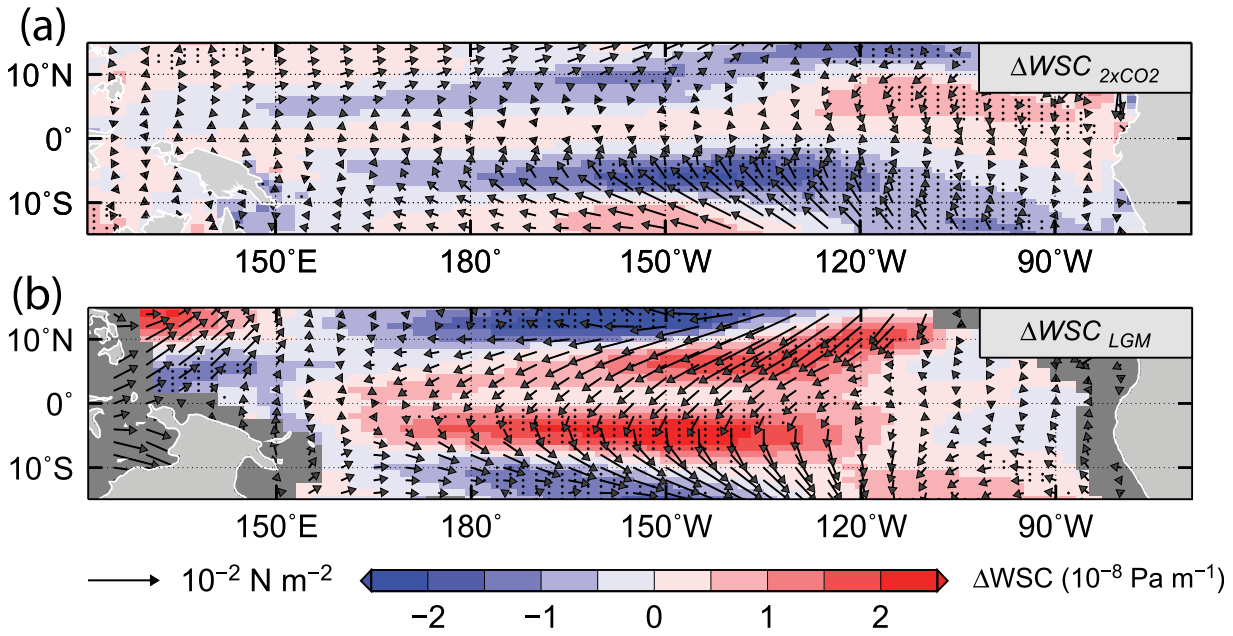

Figure 8. Wind changes in response to 2xCO2 and LGM forcing. Multimodel mean change in surface wind stress (arrows) and curl (WSC, colors) simulated by six coupled general circulation models (GCMs) in response to (a) doubling of atmospheric CO_2 (2xCO2) and (b) LGM forcing. Stippling is as in Figure 1.

the LGM experiment in agreement with the changes in the Walker circulation diagnosed from the east-west SLP difference (Figure 4d, blue dots). Changes in $\langle \tau^x \rangle$ and dSLP are highly correlated on ENSO timescales because the zonal momentum balance is dominated by the pressure gradient (i.e., dSLP) and the transfer of momentum into the ocean surface (i.e., τ^x) [*Clarke and Lebedev*, 1996]. However, in some of the models (FGOALS-g1.0, MIROC3.2) the percent change in the east-west SLP difference (dSLP) does not translate into the same magnitude of change in zonal trade winds (Figure 7). This suggests that in these models the zonal momentum balance may be influenced by processes that are negligible on ENSO timescales, such as nonlinear advection of zonal momentum and changes in boundary layer depth. Moreover, the lack of a one-to-one scaling could become a limitation to estimating the change in dSLP from the change in $\langle \tau^x \rangle$ inferred from the tilt of the thermocline as we discuss in section 5.2.

[33] Ocean changes may also result from changes in the curl of the surface wind stress (WSC), even in the absence of changes in the zonal component of the winds. The weakening of the equatorial trade winds in the 2xCO2 experiments results in a pattern of positive (negative) WSC north (south) from the equator (Figure 8a, colors). The off-equatorial Sverdrup response to this anomalous WSC drives divergence of mass from the equator, shoaling the equatorial thermocline as a result [*Vecchi and Soden*, 2007a; *DiNezio et al.*, 2009]. In contrast, in the LGM experiments, the equatorial WSC changes are dominated by a positive WSC anomaly centered on the equator (Figure 8b, colors), associated with the curvature of the cross-equatorial winds. This WSC anomaly results mostly from the meridional component of the wind changes. The Sverdrup response to this WSC forcing consists of cross-equatorial northward transport, which may deepen the equatorial thermocline due to convergence of mass on the equator, even in the absence of stronger zonal winds.

[34] The cross-equatorial winds in the central Pacific were a feature of early LGM experiments using slab ocean models [e.g., *Andreasen et al.*, 2001]. This study attributed the cross-equatorial winds to the response of the global Hadley cell to stronger cooling in the Northern Hemisphere (NH). Modeling studies have shown that the meridional position of the ITCZ; hence the location of the ascending branch of the Hadley cell, is sensitive to interhemispheric gradients in cooling/warming [*Broccoli et al.*, 2006; *Chiang and Bitz*, 2005] and radiative forcing [*Yoshimori and Broccoli*, 2009], for instance, shifting southward as the northern extratropics cool.

[35] All six models analyzed here simulate cross-equatorial winds, but not all the models simulate an anomalous cross-equatorial global Hadley circulation in the LGM experiment (not shown). The only robust LGM change is an equatorward shift of the poleward flank of the NH Hadley cell, but its impact on the equatorial circulation appears negligible. Moreover, not all the models with an anomalous cross-equatorial global Hadley circulation simulate an interhemispheric contrast in cooling (see CCSM3.0 and HadCM3M2 in Figure 9d). However, all the models simulate a deepened Aleutian low suggesting that the cross-equatorial trade winds could be driven by the changes in North Pacific circulation. In the NH tropics the surface wind stress vectors reflect the anticyclonic circulation associated with the equatorward shift of the North Pacific subtropical high (not shown), which is deflected into the SH close to the equator. In the absence of Coriolis force, the anomalous high pressure associated with the shift of the high could drive the cross-equatorial flow into the SH. The implications of the

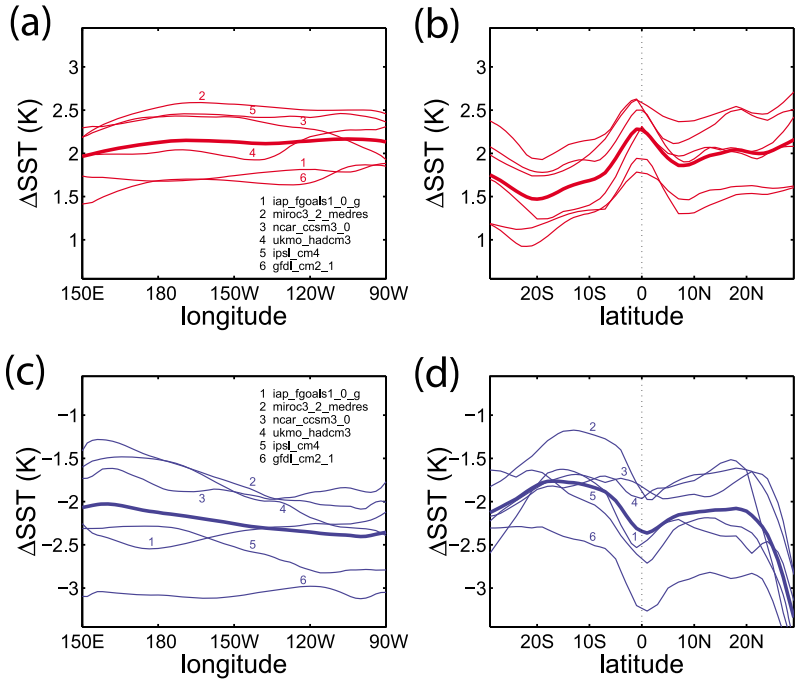

Figure 9. Signature of tropical Pacific warming and cooling. Change in surface temperature in the equatorial Pacific in response to (a) 2xCO2 (red) and (c) LGM forcing (blue) simulated by six coupled GCMs (thin lines) and their multimodel mean (solid line). The equatorial changes (Figures 9a and 9c) are averaged over 5°S and 5°N. Zonal mean change in surface temperature in the tropical Pacific in response to (b) CO_2 doubling and (d) LGM forcing simulated by six models (thin lines) and multimodel mean (solid line). The zonal mean changes (Figures 9b and 9d) are averaged from 150°E to 90°W.

changes in surface wind stress for the ocean circulation are discussed in section 5.

5. Ocean Response to Changes in the Walker Circulation

5.1. Sea Surface Temperature

[36] El Niño- or La Niña-like SST patterns are generally interpreted as a weaker or stronger Walker circulation in GCM experiments [e.g., *Knutson and Manabe*, 1995; *Meehl et al.*, 2007], observations [e.g., *Cane et al.*, 1997], or paleoreconstructions of tropical Pacific climate changes [*Lea et al.*, 2000; *Koutavas et al.*, 2002]. Recent studies indicate that an enhanced equatorial warming (EEW) pattern is a more robust indication of a weaker Walker circulation in AGW experiments rather than the zonal gradient [*Liu et al.*, 2005; *DiNezio et al.*, 2009]. The six models analyzed here simulate EEW evidenced in the zonal mean warming (Figure 9b) but do not agree in the changes in the zonal gradient (Figure 9a).

[37] The opposite response, enhanced equatorial cooling (EEC), would indicate a stronger Walker circulation in LGM experiments. However, the LGM experiments do not exhibit a consistent relationship between EEC and a stronger Walker circulation. In contrast to the 2xCO2 experiments, two different patterns associated with changes in the winds can be identified in the zonal (Figure 9c) or meridional (Figure 9d) SST changes: (1) EEC resulting from increased ocean dynamical cooling due to stronger zonal currents in response to a stronger Walker circulation and (2) a north-south gradient in cooling resulting from enhanced (reduced) ocean cooling in the NH (SH) equatorial Pacific due to the anomalous northward meridional currents forced by the anomalous cross-equatorial winds.

[38] Two out of the four models with a stronger Walker circulation simulate an EEC pattern. In the remaining two models, the interhemispheric gradient may dominate over the EEC response despite the stronger equatorial trade winds. In FGOALS-g1.0 and IPSL-CM4, the ocean response to cross-equatorial winds is much weaker compared with the zonal changes, especially in FGOALS-g1.0, which shows the largest increase (20%) in equatorial zonal wind stress, explaining why the EEC pattern is evident in the SST changes, just opposite to the 2xCO2 experiments. In contrast, CCSM3.0, a model that simulates a stronger Walker circulation, exhibits unchanged zonal and meridional equatorial gradients in SST, and no indication of EEC. MIROC3.2 simulates a 30% stronger Pacific Walker circulation (measured by the east-west SLP difference between the western and eastern Pacific), but the trade winds strengthen by just 10%, perhaps explaining why the EEC pattern cannot be distinguished from the interhemispheric pattern.

5.2. Thermocline

[39] In both 2xCO2 and LGM experiments, the changes in subsurface thermal structure on the equatorial Pacific exhibit changes related to changes in wind forcing; however, the link is not straightforward because the equatorial thermocline responds to both dynamical and thermodynamical forcing, local and remote. The six models simulate robust changes in

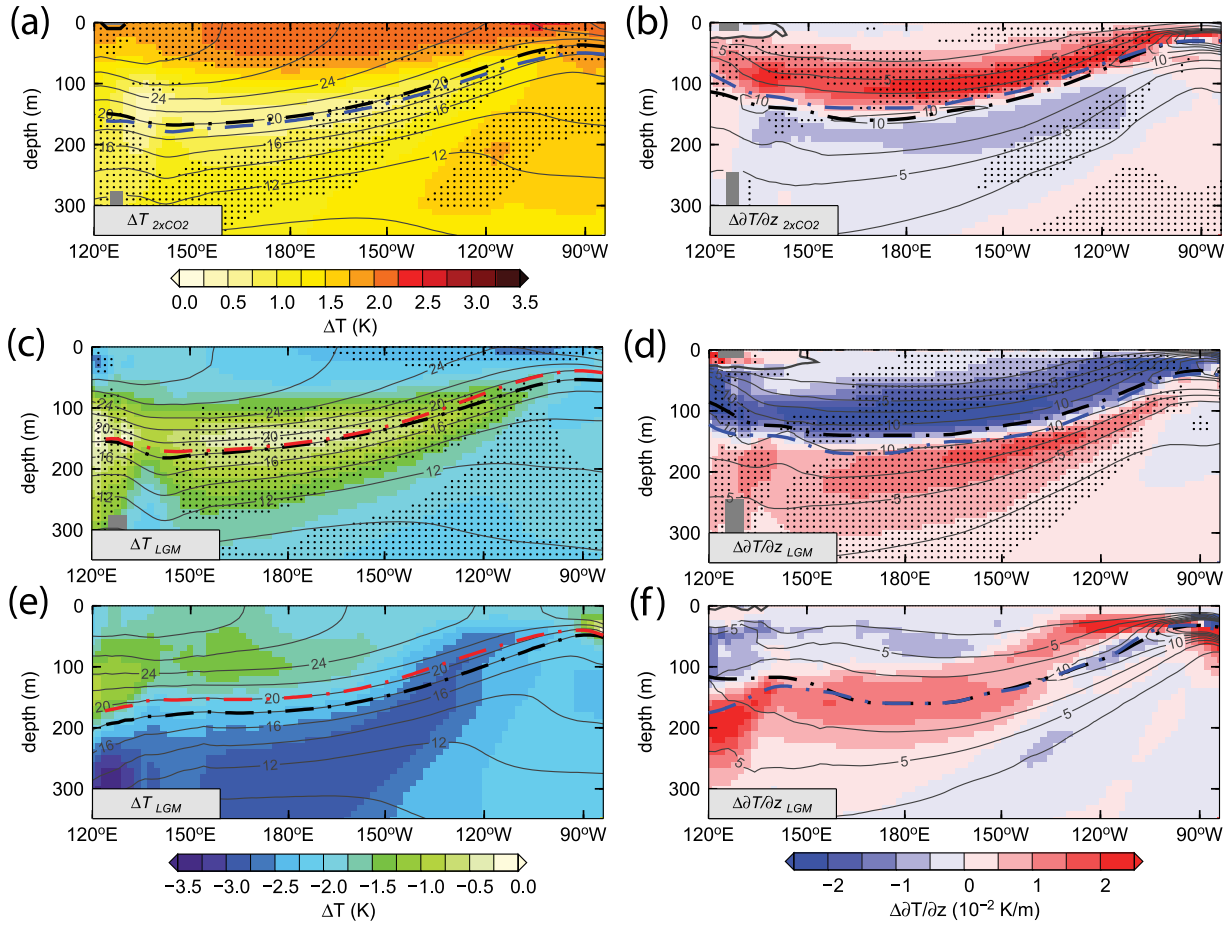

Figure 10. Response of the equatorial thermocline to 2xCO2 and LGM forcing. Multimodel change in equatorial Pacific Ocean (a) temperature and (b) vertical temperature gradient ($\partial T/\partial z$) simulated by six coupled GCMs in response to 2xCO2 forcing. Multimodel change in equatorial Pacific ocean (Figures 10c and 10e) temperature and (Figures 10d and 10f) $\partial T/\partial z$ simulated by (Figures 10c and 10d) MIROC3.2, FGOALS-g1.0, and IPSL-CM4 (three-model ensemble mean) and by (Figures 10e and 10f) CCSM3.0 in response to LGM forcing. These four models simulate a stronger Walker circulation in response to LGM forcing. The changes in CCSM3.0 are shown separately because this model's subsurface response is substantially different than that of the remaining three models with a stronger Walker circulation. Stippling is as in Figure 1. In Figures 10a, 10c, and 10e the dash-dotted lines indicate the 20°C (2xCO2) and 18°C (LGM) isotherms in the control (black) and forced (red) experiments. In Figures 10b, 10d, and 10f the dash-dotted lines indicate the depth of the thermocline, i.e., the maximum of $\partial T/\partial z$, in the control (black) and forced (blue) experiments. The equatorial sections are averaged over the 2°S and 2°N latitude band. Contours show multimodel annual mean temperature and $\partial T/\partial z$ simulated in the control experiment. CI = 2 K (temperature) and CI = 2.5 10^{-2} K m^{-1} ($\partial T/\partial z$).

thermal structure in the equatorial Pacific in response to 2xCO2, with a minimum in warming in the western Pacific at depths of about 150 m where the thermocline is located (Figure 10a). The changes in thermal stratification, $\partial T/\partial z$, in response to 2xCO2 forcing (Figure 10b) show a sharper thermocline and a zonal mean shoaling of the thermocline (Figure 10b, reds).

[40] The depth of the 20°C isotherm, Z_{20}, is often used to explore interannual changes in the depth of the thermocline, Z_{TC}, in the tropical Pacific. However, this is problematic in multimodel climate change analyses because (1) the isotherm that is representative of the thermocline varies from model to model and (2) the isotherms that are representative of the thermocline will change as the climate warms or cools. A more general method is to define Z_{TC} as the vertical location of the maximum vertical temperature gradient. To illustrate this difference we plot Z_{20} in the control and 2xCO2 experiments overlaid on the temperature changes (Figure 10a, blue and black dashed lines) and Z_{TC} in the control and 2xCO2 experiments overlaid on the $\partial T/\partial z$ changes (Figure 10b, blue and black dashed lines). The changes in Z_{20} are quite different from the Z_{TC} changes, with changes in Z_{20} having a somewhat larger signal in the eastern basin, whereas the simulated Z_{TC} changes are larger in the western Pacific.

[41] The 2xCO2 changes in Z_{TC} (Figure 10b, dashed lines) are consistent with the equilibrium response to weaker zonal winds, consisting of a zonal mean shoaling of the thermocline in response to the curl of the wind, in addition to the relaxation of the thermocline tilt [*DiNezio et al.*, 2010; *Clarke*, 2010]. In the eastern Pacific, the zonal mean shoaling of the equatorial thermocline opposes the deepening due to a reduced tilt resulting in negligible changes. The two effects contribute to a shoaling of the thermocline in the western Pacific, bringing cooler waters upward, thus explaining the minimum in subsurface warming (Figure 10a).

[42] In contrast, the LGM changes in the equatorial thermocline do not exhibit a robust minimum in cooling in the western Pacific expected from a stronger Walker circulation. Three out of the four models that simulate a stronger Walker circulation in the LGM experiments simulate a minimum in subsurface cooling in the western Pacific (Figure 10c) consistent with a long-term response of the thermocline to stronger trade winds, much like the subsurface minimum in warming in the 2xCO2 experiments (Figure 10a). The remaining model, CCSM3.0, simulates a near opposite response, with a subsurface maximum in cooling with a magnitude about 1 K larger than the surface (Figure 10e). The fact that the subsurface cooling is greater than the tropical mean surface cooling strongly suggests that this anomaly originated in the extratropics, where surface cooling is stronger (Figure 1b). Nonetheless, this model simulates a stronger thermocline tilt (Figure 10f, dashed lines) in equilibrium with the stronger wind forcing in this model (Figure 7, blue dot number 3).

[43] In models with a stronger LGM Walker circulation the vertical temperature gradient $\partial T/\partial z$, exhibits increased (decreased) thermal stratification below (above) the thermocline (Figure 10d). These changes in stratification reflect a zonal mean deepening of the thermocline, which according to equatorial adjustment theory, occurs once Rossby waves adjust the equatorial ocean establishing a Sverdrup response to the WSC changes [*Vecchi et al*., 2006; *Vecchi and Soden*, 2007a; *DiNezio et al.*, 2010; *Clarke*, 2010]. In the eastern Pacific, this response opposes the shoaling due to a stronger tilt resulting in negligible Z_{TC} changes there. This is clearly shown by the dash-dotted lines in Figure 10d indicating Z_{TC} in the control (black) and LGM (blue) climates. This has implications for the coupled response, because in contrast with La Niña events, the thermocline does not shoal in central and eastern Pacific. Therefore the positive feedback loop between winds, SST, and thermocline depth (i.e., the Bjerknes feedback) breaks down.

[44] In the LGM experiments the depth of the 18C isotherm, Z_{18} (Figure 10c, dash-dotted lines) does not change in the west due to competing effects between the surface cooling shoaling this isotherm, and the dynamical response to the winds, deepening the thermocline. In the eastern Pacific, the shoaling of Z_{18} is due to the surface cooling, because the thermocline changes are negligible there. In general, due to competing dynamical and thermodynamical effects the changes in Z_{TC} do not agree with the changes in Z_{18}, or any other isotherm that lies the in thermocline in the present climate.

[45] Apart from the minima in warming or cooling in the western Pacific, the 2xCO2 changes in temperature and thermal stratification exhibit warming that is intensified near the surface. In contrast, the LGM experiments show cooling that is more uniformly distributed throughout the water column, with no differences between the surface and the deep ocean. The intensification of the 2xCO2 ocean warming is not unexpected because the deep ocean takes centuries to adjust to the surface forcing [*Hewitt et al.*, 2003]. The AGW experiments are too short to achieve a completely equilibrated deep ocean. In contrast, much longer integrations are performed to ensure that the deep ocean is equilibrated in the LGM experiments. This explains why the LGM experiments do not exhibit surface intensified cooling or a sharper thermocline. In other words, in the 2xCO2 experiments, the surface enhanced warming can be thought of as a transient response as proposed by *DiNezio et al.* [2009] and not as a result of anomalies subducted from the extratropics as proposed by *Seager and Murtugudde* [1997]. Moreover, the lack of anomalous stratification in the LGM experiments, suggests that the *ocean dynamical thermostat* mechanism proposed by *Clement et al.* [1996] does not play a dominant role in the response of the equatorial Pacific to LGM forcing. In contrast, this mechanism operates in the AGW experiments due to the transient increase in stratification, but without driving the equatorial Pacific into a La Nina-like state [*DiNezio et al.*, 2009, 2010].

[46] Another difference arising from the different time scales of the AGW and LGM responses is that changes from remote areas of the ocean have sufficient time to reach the equatorial Pacific in the LGM experiments. This could explain the enhanced subsurface cooling in CCSM3.0 (Figure 10e), which could originate from surface anomalies subducted from the extra tropics. Analysis of the temperature changes suggests that this anomaly originates in the NH (not shown), in disagreement with model and observational analysis that have shown that only anomalies subducted in the SH can influence the equatorial thermocline [*Liu et al.*, 1994; *Lu et al.*, 1998; *Shin and Liu*, 2000]. The spatial features of this anomaly, which can be traced back to the NH midlatitude thermocline, suggest that is a response to the surface forcing and unlikely to be an artifact of the deep ocean adjustment. This is the only model that simulates this type of remote response, but the implications for the equatorial climate warrants further investigation of the underlying mechanisms.

[47] According to the GCM experiments neither the La Niña analog nor the EEC pattern provide a framework from which to infer LGM changes in the Walker circulation from SST proxies. For instance, in each model the relative changes in zonal SST gradient are generally uncorrelated with relative changes in the equatorial trade winds (Figure 11a) both for 2xCO2 and LGM experiments. The intermodel changes in the Z_{18} tilt, a measure of the depth of the thermocline frequently used in the paleoceanographic literature [e.g., *Andreasen and Ravelo*, 1997], are less consistent with the changes in the trade winds (Figure 11c) than the changes in Z_{TC} tilt. The changes in Z_{18} tilt are consistent with the changes in zonal winds in only three models. Among the models where the tilt of Z_{18} is not a good proxy for the trade winds, HadCM3M2 exhibits a large departure from the one-to-one relationship. In contrast, five out of the six models simulate changes in Z_{TC} tilt that are consistent with the wind changes (Figure 11b).

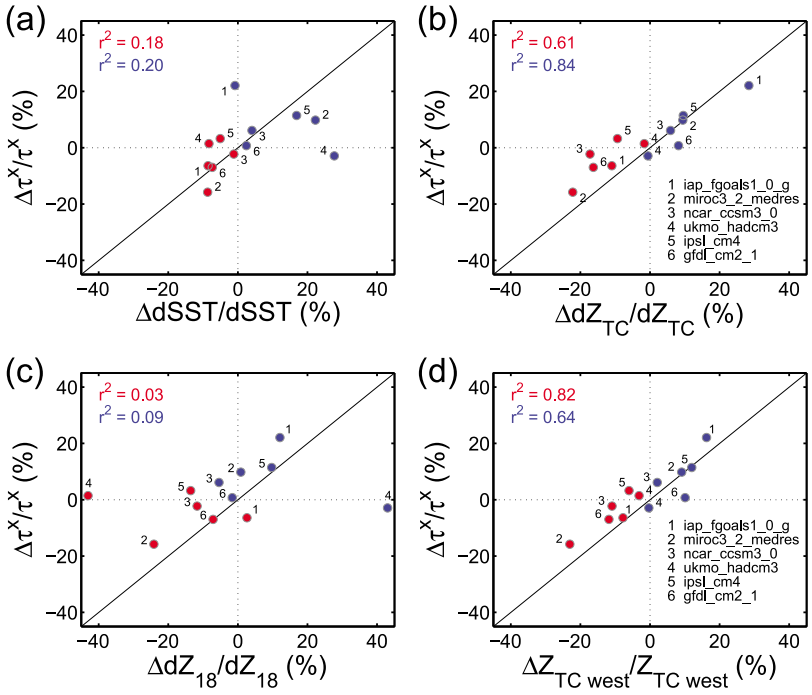

Figure 11. Ocean proxies for equatorial Pacific trade winds. Relative changes in equatorial Pacific trade winds (τ^x) in response to 2xCO2 forcing (red) and to LGM (blue) forcing versus relative change in (a) zonal sea surface temperature gradient (dSST), (b) zonal gradient of the depth of the thermocline (dZ_{TC}), (c) zonal gradient of the depth of the 18°C isotherm (dZ_{18}), and (d) depth of the thermocline in the western Pacific ($Z_{TC\ west}$). In Figures 11a–11d, the changes in τ^x, dSST, dZ_{TC}, and dZ_{18} are zonal averages over the equatorial band 2°S–2°N, 150°E–90°W. The changes in Z_{TC} on the western Pacific are averaged over 2°S–2°N, 150°E–180°.

[48] On the equator, where the Coriolis force vanishes, and in the absence of friction, the changes in thermocline tilt and zonal winds have to balance according to:

$$g' h_x = \frac{\tau^x}{\rho_0 H}, \tag{1}$$

where g' is the reduced gravity, a measure of density contrast between the upper ocean and the deep ocean, h_x is zonal gradient of the depth of thermocline, τ^x is the zonal component of the wind stress, ρ_0 is a reference density of seawater, and H is the depth of the Ekman layer. For the LGM experiments, the changes in thermocline sharpness, i.e., the maximum $\partial T/\partial z$, are negligible (not shown) because the ocean climate is fully equilibrated; thus, g' can be taken as constant. The following one-to-one relation ship between the relative changes in thermocline tilt, $\Delta h_x/h_x$, and wind stress, $\Delta\tau^x/\tau^x$, results from (1) assuming a constant Ekman layer, H:

$$\frac{\Delta h_x}{h_x} = \frac{\Delta \tau^x}{\tau^x}. \tag{2}$$

The changes in the zonally averaged zonal component of the surface wind stress and the zonally averaged tilt of the thermocline simulated by the GCMs agree with this scaling exhibiting a very close one-to-one relationship ($r^2 = 0.84$, Figure 11b, blue dots). The 2xCO2 experiments simulate an increase in thermocline sharpness, g' which according to (1) requires a smaller thermocline tilt to balance a given wind forcing. Thus, if the wind weakens, the thermocline tilt has to relax further to remain in balance with the wind. Conversely, due to the increased stratification, the thermocline tilt could relax, even in the absence of weaker winds. The GCM experiments exhibit larger (relative to the one-to-one relationship) changes in thermocline tilt than in winds consistent with this argument (Figure 11b, blue circles). Because the changes in thermocline depth are negligible in the east, the relative changes in the thermocline depth in the western Pacific also follow a one-to-one relationship with wind changes (Figure 11d), although they are still biased about the one-to-one line for the 2xCO2 case. Therefore, observational or proxy estimates of the thermocline depth in the western equatorial Pacific could provide information to constrain the changes in the Walker circulation.

5.3. Sea Surface Salinity

[49] The changes in precipitation, ΔP, simulated by all six models in response to LGM forcing (Figures 12c and 12d) are closely linked to the changes in atmospheric overturning circulation diagnosed by $\Delta\omega_{500}$ (Figures 12a and 12b). Precipitation changes are both due to radiative, thermodynamical, and dynamical processes [*Held and Soden*, 2006]. The former is responsible for a tropical mean precipitation reduction (increase) in precipitation by about 2.7% K^{-1} (1.5% K^{-1}) associated with tropical mean cooling (warming) (Figure 4b), but in some regions precipitation increases due to changes in circulation. In the LGM experiments, precip-

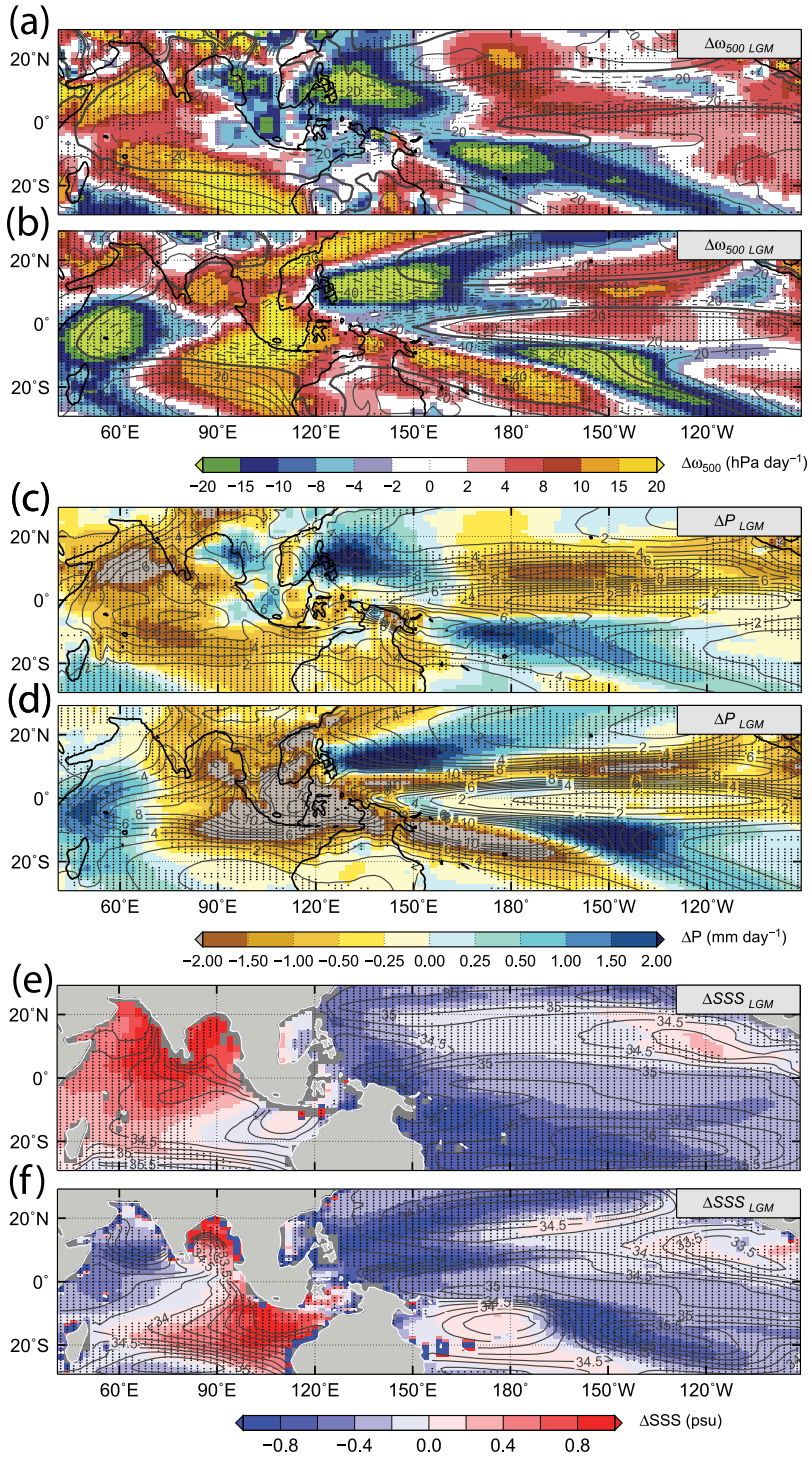

Figure 12. LGM changes in atmospheric overturning circulation, precipitation, and sea surface salinity. Two-model ensemble mean change in (a and b) midtropospheric vertical velocity ($\Delta\omega_{500}$), (c and d) precipitation (ΔP), and (e and f) sea surface salinity (ΔSSS) simulated by coupled general circulation models (GCMs) in response to LGM forcing. Figures 12a, 12c, and 12e correspond to the GCMs that simulate a much stronger (30%) Pacific Walker circulation in the LGM experiment (FGOALS-g1.0 and MIROC3.2). Figures 12b, 12d, and 12f correspond to the GCMs that simulate no changes in the Pacific Walker circulation in the LGM experiment (HadCM3M2 and GFDL-CM2.1). Stippling indicates where the two models agree in the sign of the changes. Contours show multimodel annual mean fields simulated in the control experiment. Contour intervals are 10 hPa d^{-1}, 1 mm d^{-1}, and 0.2 psu for ω_{500}, precipitation, and SSS, respectively. Note that the $\Delta\omega_{500}$ and ΔP color scales are not linear.

Table 2. Spatial Correlation Coefficient Between the Changes in Midtropospheric Vertical Velocity ($\Delta\omega_{500}$), Precipitation (ΔP), Evaporation Minus Precipitation [$\Delta(E - P)$], and Sea Surface Salinity (ΔSSS) Over the Tropical Indo-Pacific (40°E–90°W, 25°N–25°N)

Model	$r(\Delta\omega_{500}, \Delta P)$ 40°E–90°W, 25°S–25°N	$r(\Delta(E - P), \Delta P)$ 40°E–90°W, 25°S–25°N	$r(\Delta P, \Delta\text{SSS})$ 40°E–90°W, 25°S–25°N
FGOALS-g1.0	−0.74	−0.98	−0.31
MIROC3.2	−0.86	−0.98	−0.56
CCSM3.0	−0.82	−0.95	−0.67
HadCM3M2	−0.89	−0.99	−0.51
IPSL-CM4	−0.60	−0.97	−0.12
GFDL-CM2.1	−0.63	−0.98	−0.40
Multimodel	−0.78	−0.97	−0.47

itation increases in regions where ascending motion increases ($\Delta\omega_{500} < 0$), such as the SPCZ, and decreases in regions where subsidence increases ($\Delta\omega_{500} > 0$), such as the central and eastern Pacific. The spatial correlation between the multimodel mean $\Delta\omega_{500}$ and ΔP over the tropical Indo-Pacific is –0.75 ± 0.12 with values ranging from −0.6 to −0.89 (Table 2) confirming that the spatial patterns of $\Delta\omega_{500}$ and ΔP agree quite well.

[50] Substantial differences in the spatial patterns of $\Delta\omega_{500}$ and ΔP can be identified among the models. HadCM3M2 and GFDL-CM2.1 simulate large reductions of precipitation over the Maritime continent (Figure 12d) coincident with the regions with anomalous subsidence over exposed land due to lowered sea level (Figure 12b). This weakening of the ascending branch of the Walker circulation could force remote changes in the tropical circulation, such as the eastward shift in the SPCZ [*Kodama*, 1999] and the increase in ascending motion over the western Indian ocean as suggested by $\Delta\omega_{500}$ (Figure 12b). In contrast, the models that exhibit the largest (30%) strengthening of the Walker circulation (FGOALS-g1.0 and MIROC3.2) do not simulate large changes in precipitation over the Maritime continent (Figure 12c), possibly due to compensating thermodynamical (i.e., drying due to the cool surface) and dynamical (i.e., a strengthened Walker circulation) effects. Moreover, these models do not simulate the large zonal shifts in precipitation in the Indian ocean and in the SPCZ, possibly due the lack of east-west shifts in convection over the Maritime continent.

[51] The close relationship between circulation and precipitation changes suggests the possibility for detecting changes in the Walker circulation in precipitation proxies. However, the simulated patterns of precipitation change fail to translate into consistent patterns of sea surface salinity change, ΔSSS (Figures 12e and 12f), a variable that can be reconstructed from proxy data. This is not unexpected since SSS is influenced by evaporation and ocean advection, in addition to precipitation [*Stott et al.*, 2002; *Oppo et al.*, 2007]. In all models, the changes in evaporation minus precipitation, $\Delta(E - P)$, are dominated by ΔP as indicated by the large spatial correlations ($r^2 > 0.90$, Table 2) suggesting that the ΔSSS results either from changes in precipitation or from changes in ocean circulation, with a much lesser role for evaporation.

[52] The spatial correlation between the multimodel mean ΔP and ΔSSS over the tropical Indo-Pacific is −0.47 ± 0.20 with values ranging from −0.31 to −0.67 (Table 2). The fact that a large fraction of the spatial variance of ΔSSS is not explained by the $\Delta(E - P)$ suggests that changes in ocean salt advection are equally important in determining the patterns of ΔSSS in the LGM. However, some features of ΔSSS could be directly linked to ΔP. For instance the large reduction in precipitation over the Maritime Continent simulated by HadCM3M2 and GFDL-CM2.1 in the LGM experiments has a clear signature in the salinity of the southeastern Indian Ocean where SSS increases by more than 1 psu (Figure 12f). These models also simulate a fresher western Indian ocean where precipitation increases (Figure 12d). Overall these patterns indicate that SSS proxies could be used to constrain the changes in the Indian Walker circulation and shifts in the SPCZ.

6. Conclusions

6.1. Mechanisms of Tropical Pacific Climate Change

[53] Using state-of-the-art coupled GCMs we have identified three mechanisms that have a key role determining patterns of regional climate change in the tropical Pacific in response to LGM forcing:

[54] 1. Strengthening of the atmospheric overturning circulation is driven by changes in the hydrological cycle in response to tropical mean cooling (HSV mechanism).

[55] 2. Weakening of the ascending branch of the Walker circulation over the Maritime continent is associated with a reduction in convection driven by enhanced land cooling over exposed areas resulting from lower sea level.

[56] 3. Anomalous cross-equatorial winds are driven by the equatorward shift of the North Pacific subtropical high in response to a strengthening of the NH stationary wave pattern forced by both the topography of the Laurentide ice sheet.

[57] All models simulate a stronger atmospheric overturning circulation in response to tropical cooling consistent with the HSV mechanism. However, the stronger tropical circulation does not necessarily result in a stronger Pacific Walker circulation. Variations in the Pacific Walker response can be consistent with the HSV mechanism, because the constraint on the tropical overturning circulation imposed by the differential between the precipitation and humidity changes must only be satisfied in the tropical mean, allowing regional deviations to occur. Several deviations from this response are found analyzing the changes in midtropospheric vertical velocity. A departure from the HSV mechanisms is found over the Maritime continent, where the models simulate anomalous subsidence. The associated reduction in convection is likely to result from enhanced cooling over land areas exposed due to lower sea level.

[58] The HSV mechanism and the reduction in convection over exposed land drive opposing responses over the Maritime continent, explaining why the ascending branch of the Indo-Pacific Walker circulation does not strengthen in all models. Each model exhibits a difference balance between these two mechanisms, resulting in a wide range of responses. In the models where the enhanced land cooling is weakest (FGOALS-g1.0, MIROC3.2), the HSV mechanism dominates the circulation changes resulting in a stronger Pacific Walker circulation. In these models, the east-west

Table 3. Mechanisms of Tropical Pacific Climate Change in AGW and LGM Experiments

Mechanism	Signature	Experiments	Forcing/Boundary Conditions	Physics	References
HSV	Stronger (weaker) thermocline tilt in LGM (AGW) experiments	LGM and 2xCO2	Tropical cooling or warming. Not restricted to GHG forcing because tropical cooling can be driven from high latitudes.	Differential in the response of precipitation and humidity constrains the changes in the tropical overturning circulation but does not necessarily result in changes in the Walker circulation.	*Held and Soden* [2006] and *Vecchi and Soden* [2007a]
Reduced convection over the Maritime Continent	Fresher (saltier) west (east) equatorial Indian ocean	LGM	Reduced sea level	Reduction in convection over exposed land over the Maritime continent driven by enhanced land cooling.	This study
Cross-equatorial winds	Interhemispheric gradient in SST change. Deeper zonal mean thermocline forced by WSC.	LGM	NH ice sheets	Equatorward shift of the North Pacific circulation driven by a strengthening of the NH stationary wave pattern in response to both the topography of the Laurentide ice sheet and the stronger equator-to-pole temperature gradient.	*Andreasen et al.* [2001]

SLP gradient increases and so do the equatorial trade winds. In the models that simulate the strongest land cooling (HadCM3M2, GFDL-CM2.1), the reduction in convection over exposed land areas overwhelms the HSV mechanism and the ascending branch of the Indo-Pacific Walker circulation weakens. This results in a weakening of the Indian Walker circulation and an unchanged Pacific Walker circulation. The changes in circulation simulated by the remaining two models (CCSM3.0, IPSL-CM4) falls in between these two responses; however, the HSV mechanism dominates and the Pacific Walker circulation strengthens.

[59] A stronger Walker Circulation does not necessarily lead to a La Niña-like SST for the LGM tropics because the Bjerknes feedback is weak on centennial to millennial timescales. On interannual time scales, i.e., ENSO, the equatorial thermocline is not in equilibrium with changes in the trade winds. This disequilibrium is the source of the quasi-oscillatory nature of ENSO, and allows for strong coupling between winds and SSTs in the central and eastern equatorial Pacific through changes in the east-west thermocline tilt. In contrast, on the much longer LGM timescales, the oceanic response is effectively in equilibrium with the stronger trade winds. The equilibrium response consists of both a zonal mean deepening in response to the wind stress curl changes (Figure 10d), in addition to the increased thermocline tilt due to strengthened zonal stress (Figure 11b). These processes oppose in the eastern basin resulting in negligible changes in thermocline depth, thereby limiting the coupling between wind and SST changes. The weaker Bjerknes feedback allows other processes, such zonal advection or clouds, to influence SST *locally*, resulting in patterns of LGM cooling that do not need to be ENSO-like. This has implications for the seasonality of the cooling, which does not need to be tied to the seasonality of upwelling, as in the ENSO analogy. The lack of amplification via the Bjerknes feedback allows other processes, such as advection by zonal or meridional currents, to influence the annual cycle of the cold tongue.

[60] The coupled GCMs analyzed here suffer from a common bias in the tropical Pacific where they simulate the cold tongue extending too far westward, or conversely, a WPWP, and associated convection on the equator, which does not extend sufficiently eastward compared with observations [*de Szoeke and Xie*, 2008]. The lack of ascending motion off the coast of the Maritime continent in the western equatorial Pacific could make the Walker circulation too sensitive to changes in land-sea distribution. This could explain why in HadCM3M2 and GFDL-CM2.1, which simulate subsidence and dry conditions extending excessively westward in the control experiment (Figure 12b, contours), the Walker circulation does not respond following the HSV mechanism. In contrast, CCSM3.0, a model where the eastward extension of the WPWP is more realistic, simulates stronger (weaker) convection east from (over) the Maritime Continent resulting in a stronger Pacific Walker circulation.

[61] The changes in surface winds associated with these three mechanisms drive changes in the ocean, which in general result in lack of robust and unambiguous signals. The signature of the SST changes best exemplifies this case because SST is influenced by myriad ocean and atmospheric processes. In contrast, the change in the tilt of the equatorial thermocline has a more straightforward relationship with the changes in equatorial trade winds and the Walker circulation. This relationship results from fundamental physics of the equilibrium response of the equatorial ocean to changes in wind forcing, explaining why the GCMs simulate a robust and consistent relationship between these two variables. The changes in the Walker circulation also have a clear signature on the precipitation changes, but these changes fail to translate into a signature in ocean salinity because other processes, such as changes in advection of salt by ocean currents, influence salinity as well. Table 3 summarizes these mechanisms, their physics, link with different LGM forcing, and robust ocean response.

6.2. Implications for Detection in Proxy Data

[62] Based on the model responses we hypothesize that during the LGM climate, the Pacific branch of the Walker

circulation strengthened via the HSV mechanism, and the Indian branch weakened due to reduced convection over exposed land. These hypotheses can be tested using thermocline and salinity proxies, respectively. Furthermore, our results indicate that SST proxies cannot be used to unambiguously constrain the sign of the response of the Pacific Walker circulation to LGM because the Bjerknes feedback is not active on climate change timescales [*Vecchi et al.*, 2006; *DiNezio et al.*, 2010; *Clarke*, 2010].

[63] Proxy estimates of thermocline changes during the LGM suggest a stronger tilt [*Andreasen and Ravelo*, 1997]. However, they used Z_{18} in the calibration of their method because this measure of the thermocline showed better correlations with the microfossil assemblages for the present climate than Z_{TC}. The analysis of the GCM experiments indicate that competing dynamical and thermodynamical processes influence the thermal structure of the upper ocean; therefore, the changes in the thermocline do not follow the changes in the depth of the 18°C isotherm, or any other isotherm that lies the in thermocline in the present climate. However, the estimates of the LGM could still capture real thermocline changes because the assemblages also exhibit significant correlations with Z_{TC}.

[64] The unmistakable subsurface temperature changes in the western Pacific simulated by the GCMs represent the strongest LGM signal associated with the changes in the Walker circulation. A recent study comparing paleotemperatures derived using Mg/Ca ratios from surface-dwelling versus thermocline dweller planktonic foraminifera provides some evidence for this signal [*Xu et al.*, 2010]. The data from a core located off the Celebes Sea (MD06-3067), where the large-scale thermocline changes driven from the western equatorial Pacific could influence the local thermocline, suggest no changes in the temperature of the thermocline between the present and the LGM, despite large cooling at the surface. The lack of subsurface cooling is consistent with the three models that simulate a deeper thermocline due to a stronger Walker circulation. More estimates from cores from the western equatorial Pacific are needed to confirm this result.

[65] The changes in thermocline are subtler in the Indian Ocean because the tilt changes required to balance the changes in the trade winds are commensurate with the basin width, which is one third of that of the Pacific. However, the patterns of the simulated SSS changes over the Indian Ocean reflect changes in precipitation and circulation. For instance, the changes in SSS simulated by HadCM3M2 and GFDL-CM2.1 (Figure 12f) are well correlated with the changes in precipitation (Figure 12d) that are driven by the weakening of the Indian Walker circulation (Figure 12b). Thus, a weakening of the east-west SSS contrast would provide evidence for a weaker Indian Walker circulation in response to suppressed convection over the Sunda shelf during the LGM.

[66] Terrestrially based precipitation proxies, such as lake levels or water isotope changes inferred from speleothems or plant leaf waxes, could be used to constrain the sensitivity of the Walker circulation to LGM forcing. The simulations indicate that there are regions where precipitation changes are more strongly governed by circulation changes. One of these regions is Borneo, where the two models with an unchanged Walker circulation simulate a strong drying associated with the reduction in convection over the Sunda Shelf. This response also leads to an eastward shift of the SPCZ, which could also be constrained by precipitation proxies over islands in the Southwestern Pacific.

[67] Proxies of continental versus ocean cooling can also help to constrain the changes in the Walker circulation suggested by the LGM experiments. According to the PMIP2 models, the magnitude of the simulated cooling over exposed land areas of the Maritime continent is about the same magnitude than the cooling over other continental areas of the SH, such as tropical South America or Australia. Proxies of the LGM also suggest enhanced continental cooling [e.g., *Broccoli*, 2000]; thus, the small differential in land-sea cooling simulated by FGOALS-g1.0 may be unrealistic. MIROC3.2 does not use an LGM land mask explaining the lack of enhanced cooling. In the models where the Walker circulation does not strengthen (GFDL-CM2.1 and HadCM3M2) ascending motion is confined to the Maritime continent in the control climate due to an excessive cold tongue bias in the control climate. Note that the solid line indicating the boundary between the ascending from the descending vertical motion is further west in these models in Figure 5). Because the strengthening due to the HSV occurs over ocean, the lack of convective areas over the ocean could explain these models are more sensitive to the reduction in convection over the Sunda Shelf. The issues are less acute in the LGM changes simulated by CCSM3.0 and IPSL-CM4. Despite the fact that these two models simulate quite different changes in the subsurface ocean temperature (Figures 12c and 12e) and the zonal and meridional SST patterns (Figures 11c and 11d); both models simulate changes in the tilt of the thermocline that follow a one-to-one relationship with the changes in the trade winds (Figure 11c). This shows that changes in the tilt of the equatorial thermocline can give an unequivocal signal of the changes in the Walker circulation.

6.3. Constraining the Sensitivity of the Walker Circulation to GHG Forcing Using Proxies of the LGM

[68] Because the LGM simulations suggest that the Walker circulation may be sensitive to both tropical cooling and the changes in the geography of the Maritime Continent, the response of the LGM tropics may not simply be an opposite analog for future AGW. Thus, if proxies of the thermocline provided evidence of a stronger tilt during the LGM, this should be unambiguously interpreted as a stronger Walker circulation, even if SST proxies did not show a La Niña-like pattern. Furthermore, models indicate that stronger trade winds are possible even with an unchanged (e.g., CCSM3.0) or a weakened SST gradient (FGOALS-g1.0). Thus, proxy evidence for a stronger thermocline tilt and weaker SST gradient would further strengthen the argument that the Walker circulation was stronger during the LGM due to tropical mean cooling as predicted by the HSV mechanism.

[69] This interpretation of proxy evidence would constrain the sign of the response due to the HSV mechanism, but not the magnitude. Constraining the magnitude of the sensitivity of the Walker circulation to cooling is more difficult. Fractional changes in thermocline tilt and trade winds follow a very close one-to-one relationship (Figure 11b); however, the changes in the trade winds do not scale one to one with the east-west SLP difference in the Pacific basin (Figure 7). Moreover, estimating the sensitivity of the Walker circulation

to tropical mean cooling using LGM data would be irremediable influenced by the changes over the Maritime continent. Because the reduction in convection due to exposed land weakens the Walker circulation, an LGM-based estimate would underestimate of the sensitivity to pure tropical cooling/warming. However, a stronger thermocline tilt during the LGM should be unambiguously interpreted as evidence that the Walker circulation is sensitive to changes in tropical mean temperature.

6.4. Implications for Model-Data Comparisons

[70] An important conclusion from analyzing and comparing 2xCO2 and LGM experiments is that the same current state-of-the-art coupled climate models agree in projections of future climate change in response to GHG forcing, but simulate diverging, even opposing, responses to LGM forcing. This is not surprising because the LGM forcing is substantially more complex, including several radiative, such as GHGs and albedo, and nonradiative, such as orographic and land surface changes. In some cases, such as the ascending branch of the Walker circulation, the response to the different forcing interfere, resulting in a wide range of responses. The complexity of the tropical climate changes suggested by the numerical experiments renders the LGM a challenging target, but ultimately, a useful benchmark to evaluate the ability of climate models to represent specific regional circulation features in climates radically different from the present. Substantial progress on both unbiased model simulations and robust estimations of the LGM climate using multiple proxies is required for this effort to bear fruit.

[71] **Acknowledgments.** We acknowledge the international modeling groups participating in PMIP2 and CMIP3, and NOAA/GFDL for providing their data for analysis, the Laboratoire des Sciences du Climat et de l'Environnement for collecting and archiving the LGM data, and the Program for Climate Model Diagnosis and Intercomparison (PCMDI) and the IPCC Data Archive at IPCC Data Archive at Lawrence Livermore National Laboratory (LLNL) for archiving the AGW data. The PMIP2/MOTIF Data Archive is supported by CEA, CNRS, the EU project MOTIF, and the Programme National d'Etude de la Dynamique du Climat. PCMDI and the IPCC Data Archive at LLNL are supported by the Office of Science of the U.S. Department of Energy. We thank David Lea and one anonymous reviewer for comments that helped improve the manuscript; Jean-Yves Peterschmitt, Michael Erb, and Gary Strand for facilitating access to output from the LGM experiments; and Jay Harris for invaluable technical support. This research was carried out in part under the auspices of the Cooperative Institute for Marine and Atmospheric Studies (CIMAS), a Joint Institute of the University of Miami and NOAA, Cooperative Agreement NA17RJ1226. P. N. DiNezio and A. Clement were supported by NSF Paleoclimate program grant ATM0902926.

References

Andreasen, D. H., and A. C. Ravelo (1997), Tropical Pacific Ocean thermocline depth reconstructions for the Last Glacial Maximum, *Paleoceanography*, *12*, 395–414, doi:10.1029/97PA00822.

Andreasen, D. H., A. C. Ravelo, and A. J. Broccoli (2001), Remote forcing at the Last Glacial Maximum in the tropical Pacific Ocean, *J. Geophys. Res.*, *106*, 879–897, doi:10.1029/1999JC000087.

Bakun, A., and S. J. Weeks (2008), The marine ecosystem off Peru: What are the secrets of its fishery productivity and what might its future hold?, *Prog. Oceanogr.*, *79*, 290–299, doi:10.1016/j.pocean.2008.10.027.

Braconnot, P, et al. (2007), Results of PMIP2 coupled simulations of the mid-holocene and Last Glacial Maximum—Part 1: Experiments and large-scale features, *Clim. Past*, *3*, 261–277, doi:10.5194/cp-3-261-2007.

Broccoli, A. J. (2000), Tropical cooling at the Last Glacial Maximum: An atmosphere-mixed layer ocean model simulation, *J. Clim.*, *13*(5), 951–976, doi:10.1175/1520-0442(2000)013<0951:TCATLG>2.0.CO;2.

Broccoli, A. J., K. A. Dahl, and R. J. Stouffer (2006), Response of the ITCZ to Northern Hemisphere cooling, *Geophys. Res. Lett.*, *33*, L01702, doi:10.1029/2005GL024546.

Cane, M. A., A. C. Clement, A. Kaplan, Y. Kushnir, D. Pozdnyakov, R. Seager, S. E. Zebiak, and R. Murtugudde (1997), Twentieth century sea surface temperature trends, *Science*, *275*, 957–960, doi:10.1126/science.275.5302.957.

Chiang, J. C. H., and C. M. Bitz (2005), Influence of high latitude ice cover on the marine Intertropical Convergence Zone, *Clim. Dyn.*, *25*, 477–496, doi:10.1007/s00382-005-0040-5.

Clarke, A. J. (2010), Analytical theory for the quasi-steady and low-frequency equatorial ocean response to wind forcing: The "tilt" and "warm water volume" modes, *J. Phys. Oceanogr.*, *40*(1), 121–137, doi:10.1175/2009JPO4263.1.

Clarke, A. J., and A. Lebedev (1996), Long-term changes in the equatorial Pacific trade winds, *J. Clim.*, *9*, 1020–1029, doi:10.1175/1520-0442(1996)009<1020:LTCITE>2.0.CO;2.

Clement, A. C., R. Seager, M. A. Cane, and S. E. Zebiak (1996), An ocean dynamical thermostat, *J. Clim.*, *9*, 2190–2196, doi:10.1175/1520-0442(1996)009<2190:AODT>2.0.CO;2.

Delworth, T. L., et al. (2006), GFDLs CM2 global coupled climate models. Part I: Formulation and simulation characteristics, *J. Clim.*, *19*, 643–674, doi:10.1175/JCLI3629.1.

de Szoeke, S. P., and S.-P. Xie (2008), The tropical eastern Pacific seasonal cycle: Assessment of errors and mechanisms in IPCC AR4 coupled ocean-atmosphere general circulation models, *J. Clim.*, *21*, 2573–2590, doi:10.1175/2007JCLI1975.1.

DiNezio, P. N., A. C. Clement, and G. A. Vecchi (2010), Reconciling differing views of tropical Pacific climate change, *Eos Trans. AGU*, *91*(16), 141–142, doi:10.1029/2010EO160001.

DiNezio, P., A. Clement, G. A. Vecchi, B. J. Soden, B. Kirtman, and S.-K. Lee (2009), Climate response of the equatorial Pacific to global warming, *J. Clim.*, *22*, 4873–4892, doi:10.1175/2009JCLI2982.1.

Farrera, I., et al. (1999), Tropical climates at the Last Glacial Maximum: A new synthesis of terrestrial palaeoclimate data. I. Vegetation, lakelevels and geochemistry, *Clim. Dyn.*, *15*, 823–856, doi:10.1007/s003820050317.

Gordon, C., C. Cooper, C. A. Senior, H. T. Banks, J. M. Gregory, T. C. Johns, J. F. B. Mitchell, and R. A. Wood (2000), The simulation of SST, sea ice extents and ocean heat transports in a version of the Hadley Centre coupled model without flux adjustments, *Clim. Dyn.*, *16*, 147–168, doi:10.1007/s003820050010.

Hasumi, H., and S. Emori (2004), K-1 coupled GCM(MIROC) description, *K-1 Tech. Rep. 1*, 34 pp., Cent. for Clim. Syst. Res., Univ. of Tokyo, Tokyo.

Held, I. M., and B. J. Soden (2006), Robust responses of the hydrological cycle to global warming, *J. Clim.*, *19*, 5686–5699, doi:10.1175/JCLI3990.1.

Hewitt, C. D., R. J. Stouffer, A. J. Broccoli, J. F. B. Mitchell, and P. J. Valdes (2003), The effect of ocean dynamics in a coupled GCM simulation of the Last Glacial Maximum, *Clim. Dyn.*, *20*, 203–218.

Knutson, T. R., and S. Manabe (1995), Time-mean response over the tropical Pacific to increased CO_2 in a coupled ocean–atmosphere model, *J. Clim.*, *8*, 2181–2199, doi:10.1175/1520-0442(1995)008<2181:TMROTT>2.0.CO;2.

Kodama, Y.-M. (1999), Roles of the atmospheric heat sources in maintaining the subtropical convergence zones: An aqua-planet GCM study, *J. Atmos. Sci.*, *56*, 4032–4049, doi:10.1175/1520-0469(1999)056<4032:ROTAHS>2.0.CO;2.

Koutavas, A., J. Lynch-Stieglitz, T. M. Marchitto, and J. P. Sachs (2002), El Niño-like pattern in ice age tropical Pacific sea surface temperature, *Science*, *297*, 226–230, doi:10.1126/science.1072376.

Lea, D. W., D. K. Pak, and H. J. Spero (2000), Climate impact of late Quaternary equatorial Pacific sea surface temperature variations, *Science*, *289*, 1719–1724, doi:10.1126/science.289.5485.1719.

Liepert, B. G., and M. Previdi (2009), Do models and observations disagree on the rainfall response to global warming?, *J. Clim.*, *22*, 3156–3166, doi:10.1175/2008JCLI2472.1.

Liu, Z., S. G. H. Philander, and R. C. Pacanowski (1994), A GCM study of tropical–subtropical upper-ocean water exchange, *J. Phys. Oceanogr.*, *24*, 2606–2623, doi:10.1175/1520-0485(1994)024<2606:AGSOTU>2.0.CO;2.

Liu, Z., S. J. Vavrus, F. He, N. Wen, and Y. Zhang (2005), Rethinking tropical ocean response to global warming: The enhanced equatorial warming, *J. Clim.*, *18*, 4684–4700, doi:10.1175/JCLI3579.1.

Lu, P., J. McCreary, and B. A. Klinger (1998), Meridional circulation cells and the source waters of the Pacific equatorial undercurrent, *J. Phys. Oceanogr.*, *28*, 62–84, doi:10.1175/1520-0485(1998)028<0062:MCCATS>2.0.CO;2.

MARGO Project Members (2009), Constraints on the magnitude and patterns of ocean cooling at the Last Glacial Maximum, *Nat. Geosci.*, *2*(2), 127–132, doi:10.1038/ngeo411.

Marti, O., et al. (2010), Key features of the IPSL ocean atmosphere model and its sensitivity to atmospheric resolution, *Clim. Dyn.*, *34*, 1–26, doi:10.1007/s00382-009-0640-6.

Meehl, G. A., et al. (2007), Global climate projections, in *Climate Change 2007: The Physical Science Basis*, edited by S. Solomon et al., pp. 747–845, Cambridge University Press, New York.

Mix, A. C., A. E. Morey, N. G. Pisias, and S. W. Hostetler (1999), Foraminiferal faunal estimates of paleotemperature: circumventing the no-analog problem yields cool ice age tropics, *Paleoceanography*, *14*, 350–359, doi:10.1029/1999PA900012.

Oppo, D. W., G. A. Schmidt, and A. N. LeGrande (2007), Seawater isotope constraints on tropical hydrology during the Holocene, *Geophys. Res. Lett.*, *34*, L13701, doi:10.1029/2007GL030017.

Otto-Bliesner, B. L., E. Brady, S. Shin, Z. Liu, and C. Shields (2003), Modeling El Nino and its tropical teleconnections during the glacial-interglacial cycle, *Geophys. Res. Lett.*, *30*(23), 2198, doi:10.1029/2003GL018553.

Otto-Bliesner, B. L., E. C. Brady, G. Clauzet, R. Tomas, S. Levis, and Z. Kothavala (2006a), Last Glacial Maximum and Holocene climate in CCSM3.0, *J. Clim.*, *19*, 2526–2544, doi:10.1175/JCLI3748.1.

Otto-Bliesner, B. L., R. Tomas, E. C. Brady, Z. Kothavala, G. Clauzet, and C. Ammann (2006b), Climate sensitivity of moderate and low resolution versions of CCSM3 to preindustrial forcings, *J. Clim.*, *19*, 2567–2583, doi:10.1175/JCLI3754.1.

Otto-Bliesner, B. L., et al. (2009), A comparison of PMIP2 model simulations and the MARGO proxy reconstruction for tropical sea surface temperatures at Last Glacial Maximum, *Clim. Dyn.*, *32*, 799–815, doi:10.1007/s00382-008-0509-0.

Rosenthal, Y., and A. J. Broccoli (2004), In search of paleo-ENSO, *Science*, *304*, 219–221, doi:10.1126/science.1095435.

Seager, R., and R. Murtugudde (1997), Ocean dynamics, thermocline adjustment and regulation of tropical SST, *J. Clim.*, *10*, 521–534, doi:10.1175/1520-0442(1997)010<0521:ODTAAR>2.0.CO;2.

Seager, R., Y. Kushnir, C. Herweijer, N. Naik, and J. Velez (2005), Modeling of tropical forcing of persistent droughts and pluvials over western North America: 1856–2000, *J. Clim.*, *18*, 4065–4088, doi:10.1175/JCLI3522.1.

Shin, S., and Z. Liu (2000), Response of equatorial thermocline to extratropical buoyancy forcing, *J. Phys. Oceanogr.*, *30*, 2883–2905, doi:10.1175/1520-0485(2001)031<2883:ROTETT>2.0.CO;2.

Shin, S.-I., Z. Liu, B. Otto-Bliesner, E. C. Brady, J. E. Kutzbach, and S. P. Harrison (2003), A simulation of the Last Glacial Maximum climate using the NCAR-CCSM, *Clim. Dyn.*, *20*, 127–151, doi:10.1007/s00382-002-0260-x.

Stott, L., C. Poulsen, S. Lund, and R. Thunell (2002), Super ENSO and global climate oscillations at millennial time scales, *Science*, *297*, 222–226, doi:10.1126/science.1071627.

Vecchi, G. A., and B. J. Soden (2007a), Global warming and the weakening of the tropical circulation, *J. Clim.*, *20*, 4316–4340, doi:10.1175/JCLI4258.1.

Vecchi, G. A., and B. J. Soden (2007b), Effect of remote sea surface temperature change on tropical cyclone potential intensity, *Nature*, *450*, 1066–1070, doi:10.1038/nature06423.

Vecchi, G. A., B. J. Soden, A. T. Wittenberg, I. M. Held, A. Leetmaa, and M. J. Harrison (2006), Weakening of tropical Pacific atmospheric circulation due to anthropogenic forcing, *Nature*, *441*, 73–76, doi:10.1038/nature04744.

Wentz, F. J., L. Ricciardulli, K. Hilburn, and C. Mears (2007), How much more rain will global warming bring?, *Science*, *317*, 233–235, doi:10.1126/science.1140746.

Xu, J., W. Kuhnt, A. Holbourn, M. Regenberg, and N. Andersen (2010), Indo-Pacific Warm Pool variability during the Holocene and Last Glacial Maximum, *Paleoceanography*, *25*, PA4230, doi:10.1029/2010PA001934.

Yoshimori, M., and A. J. Broccoli (2009), On the link between Hadley circulation changes and radiative feedback processes, *Geophys. Res. Lett.*, *36*, L20703, doi:10.1029/2009GL040488.

Yu, Y. Q., X. H. Zhang, and Y. F. Guo (2004), Global coupled ocean-atmosphere general circulation models in LASG/IAP, *Adv. Atmos. Sci.*, *21*, 444–455, doi:10.1007/BF02915571.

P. Braconnot, IPSL, Laboratoire de Sciences du climat et de l'environnement, CEA Saclay, Orme des Merisiers, F-91191 Gif-sur-Yvette, France.

A. J. Broccoli, Department of Environmental Sciences, Rutgers University, 14 College Farm Rd., New Brunswick, NJ 08901-8551, USA.

A. Clement, P. N. DiNezio, and B. Soden, Division of Meteorology and Physical Oceanography, RSMAS, University of Miami, 4600 Rickenbacker Causeway, Miami, FL 33149, USA. (pdinezio@rsmas.miami.edu)

B. L. Otto-Bliesner, Climate Change Research Section, CCR/CGD, NCAR, 1850 Table Mesa Dr., PO Box 3000, Boulder, CO 80307, USA.

G. A. Vecchi, Geophysical Fluid Dynamics Laboratory, NOAA, Princeton Forrestral, Campus Route 1, PO Box 308, Princeton, NJ 08542-0308, USA.